CHAPTER 2 «FORMATION OF TRANSVERSE MODES WITH A SPATIALLY INHOMOGENEOUS POLARIZATION IN A DIELECTRIC WAVEGUIDE RESONATOR»

DOI: https://doi.org/10.30525/978-9934-26-461-0-2

In many applications of THz laser radiation its state of polarization is an important parameter that determines the result of the interaction of this radiation with matter. In a number of such tasks, it is necessary to use a laser beam with axial symmetry, including polarization. In this case a laser beam with a uniform distribution of the electric field vector (the electric vector is linearly polarized and has a common direction across the entire cross section of the beam) is unacceptable. With circular polarization the parameters of the interaction of radiation with matter are averaged, which means that they are not optimal either from the point of view of minimum losses or from the point of view of maximum absorption [78]. Currently axisymmetric laser beams with radial and azimuthal radiation polarizations are of great practical interest.

The problem of its obtaining occupies an important place in the studies of axisymmetrically polarized radiation [12]. Several basic methods for solving this problem are known: use of a conical reflector or a Brewster conical window in the resonator, induced axisymmetric birefringence in the active element of a solid-state laser, Zeeman polarization effect in an axisymmetric magnetic field, extra-resonator formation of axisymmetrically polarized laser beams from beams with circular and linear polarization. All of the above methods are technically difficult or their application is limited to low-intensity radiation. Recently a direction has been developed in the optical range associated with the use of diffractive mirrors possessing high polarization selectivity. The special pattern of their relief provides the maximum Q-factor of the mode with a given direction of polarization [79]. However, these methods are oriented towards a specific type of radiation polarization.

Let us mention several papers devoted to generation, propagation and focusing of beams with various spatial polarisation of radiation in the terahertz (THz) frequency range [80–84], as well as papers [29; 31–33; 85–87], which describe methods of and approaches to forming laser beams with a required polarisation structure in this range. Nevertheless, they all pertain to the group of extracavity methods and utilize pulsed radiation emitted upon nonlinear conversion of IR femtosecond laser radiation.

In this regard, an urgent problem is the search for simple and energy-efficient intracavity methods for the formation and selection of transverse modes with a given polarization state of the output radiation in THz quantum generators.

2.1. MATHEMATICAL MODELING OF QUASI-OPTICAL LASER RESONATORS WITH DIFFRACTION MIRRORS

2.1.1. A Multi-ring Diaphragm in a Dielectric Waveguide

It is well known that TE, TM and EH modes exist in a hollow dielectric waveguide. Let's write the expressions for the transverse components of the electric field inside the waveguide ($r < a$) for the case when the radiation wavelength λ is much smaller than the waveguide radius a ($\lambda << a$) [50]:

– for TE_{0m} mode

$$E_{\varphi}^{(m)}(r,\varphi) = A_m J_1\left(u_{0m} r / a\right), \tag{2.1}$$

– for TM_{0m} mode

$$E_{r}^{(m)}(r,\varphi) = B_m J_1\left(u_{0m} r / a\right), \tag{2.2}$$

– for EH_{nm} mode (here the index n can also be negative)

$$E_{\varphi}^{(nm)}(r,\varphi) = C_{nm} J_{n-1}\left(u_{nm} r / a\right)\cos\left(n\varphi\right), \tag{2.3}$$

$$E_{r}^{(nm)}(r,\varphi) = C_{nm} J_{n-1}\left(u_{nm} r / a\right)\sin\left(n\varphi\right). \tag{2.4}$$

Here u_{nm} is the m-th root of the equation $J_{n-1}\left(u_{nm}\right) = 0$.

The constants A_m, B_m and C_{nm} can be determined from the following orthonormalization condition:

$$\int_0^{2\pi}\int_0^{a}\left(E_r^{(i)}\left(r,\varphi\right)E_r^{(j)}\left(r,\varphi\right) + E_{\varphi}^{(i)}\left(r,\varphi\right)E_{\varphi}^{(j)}\left(r,\varphi\right)\right) r dr d\varphi = \delta_{i,j}. \tag{2.5}$$

At the same time, superscripts i and j correspond to different modes and the spatial distribution of the field is determined by formulas (2.1) – (2.4). Note that, in a hollow dielectric waveguide, in addition to modes (2.1) – (2.4), there are also combined modes that represent the superposition of some modes considered above (for example, TE_{0m} + EH_{2m}) [88]. The field for such combined modes is defined as the sum of the corresponding expressions from formulas (2.1) – (2.4).

In an infinite regular hollow dielectric waveguide, all modes propagate independently. However, on inhomogeneities, the interaction of different modes and the transformation of energy from one type of mode into

another takes place. We have conducted a study of mode diffraction with an axially symmetric large-scale diaphragm consisting of metal rings. Due to the presence of axial symmetry, the angular dependence of the fields during diffraction on the diaphragm does not change. However, modes with different radial dependences of the field (with different radial indices) will interact on an axially symmetric diaphragm and transform into each other. Thus, TE_{0m} (TM_{0m}) modes can transform into modes of their own class, but with different TE_{0k} (TM_{0k}) radial indices. Similarly, EH_{nm} modes can transform into EH_{nk} modes, as well as EH_{-nk} modes, which have the same axial dependence of the fields (see formulas (2.3) – (2.4)).

In the finite-difference method in the time domain for bodies of rotation (BOR-FDTD), the investigated fields are decomposed into a series of independent angular harmonics [89]:

$$\vec{E} = \sum_{m=0}^{\infty} \left(\vec{e}_u \cos(m\varphi) + \vec{e}_v \sin(m\varphi) \right),$$
$$\vec{H} = \sum_{m=0}^{\infty} \left(\vec{h}_u \cos(m\varphi) + \vec{h}_v \sin(m\varphi) \right). \qquad (2.6)$$

This allows us to convert Maxwell's three-dimensional equations into a two-dimensional problem for independent angular modes in cylindrical coordinates ρ, z.

In this case, the renewal formulas for the field components can be easily obtained from Maxwell's equations in the cylindrical coordinate system [89; 90]. The equations for components u and v from (2.6) are identical, in the following these indices are omitted.

The renewal formulas for the electric field:

$$e_\rho\Big|_{i+1/2,k+1/2}^{n+1/2} = e_\rho\Big|_{i+1/2,k+1/2}^{n-1/2} + \frac{\Delta t}{\varepsilon \Delta z}\left(h_\varphi\Big|_{i+1/2,k}^{n} - h_\varphi\Big|_{i+1/2,k+1}^{n} \right) -$$
$$- \frac{m\Delta t / \varepsilon}{(i+1/2)\Delta r} h_z\Big|_{i+1/2,k+1/2}^{n},$$
$$e_\varphi\Big|_{i,k+1/2}^{n+1/2} = e_\varphi\Big|_{i,k+1/2}^{n-1/2} + \frac{\Delta t}{\varepsilon \Delta r}\left(h_z\Big|_{i-1/2,k+1/2}^{n} - h_z\Big|_{i+1/2,k+1/2}^{n} \right) +$$
$$+ \frac{\Delta t}{\varepsilon \Delta z}\left(h_\rho\Big|_{i,k+1}^{n} - h_\rho\Big|_{i,k}^{n} \right),$$
$$e_z\Big|_{i,k}^{n+1/2} = e_z\Big|_{i,k}^{n-1/2} + \frac{\Delta t}{\varepsilon i \Delta r}\left[\begin{array}{l} (i+1/2) h_\varphi\Big|_{i+1/2,k}^{n} - \\ -(i-1/2) h_\varphi\Big|_{i-1/2,k}^{n} + m h_\rho\Big|_{i,k}^{n} \end{array} \right]. \qquad (2.7)$$

The renewal formulas for the magnetic field:

$$h_\rho\Big|_{i,k}^{n+1} = h_\rho\Big|_{i,k}^{n} + \frac{\Delta t}{\mu\Delta z}\left(e_\varphi\Big|_{i,k+1/2}^{n+1/2} - h_\varphi\Big|_{i,k-1/2}^{n+1/2}\right) - \\ - \frac{m\Delta t}{\mu i\Delta r} e_z\Big|_{i,k}^{n+1/2},$$

$$h_\varphi\Big|_{i+1/2,k}^{n+1} = h_\varphi\Big|_{i+1/2,k}^{n} + \frac{\Delta t}{\mu\Delta z}\left(e_z\Big|_{i+1,k}^{n+1/2} - e_z\Big|_{i,k}^{n+1/2}\right) + \\ + \frac{\Delta t}{\mu\Delta z}\left(e_\rho\Big|_{i+1/2,k-1/2}^{n+1/2} - e_\rho\Big|_{i+1/2,k+1/2}^{n+1/2}\right),$$

$$h_z\Big|_{i+1/2,k+1/2}^{n+1} = h_z\Big|_{i+1/2,k+1/2}^{n} + \\ + \frac{\Delta t}{(i+1/2)\mu\Delta r}\left(\begin{array}{l} i\,e_\varphi\Big|_{i,k+1/2}^{n+1/2} - (i+1)e_\varphi\Big|_{i+1,k+1/2}^{n+1/2} + \\ + m\,e_\rho\Big|_{i+1/2,k+1/2}^{n+1/2} \end{array}\right). \quad (2.8)$$

Here, Δt, Δz and Δr are the time step and spatial (longitudinal and radial) steps, respectively. Superscript index n describes the time step index $t = n\Delta t$, subscripts i and k are spatial radial and longitudinal indices $r = i\Delta r$, $z = k\Delta z$, respectively. Formulas (2.7) – (2.8) allow to calculate the values of the field components at off-axis points ($r \neq 0$). In the case of axial points ($r = 0$), the situation is different [89]: different equations are used for different angular indices.

If $m = 0$ only

$$e_z\Big|_{0,k}^{n+1/2} = e_z\Big|_{0,k}^{n-1/2} + \frac{4\Delta t}{\varepsilon\Delta r} h_\varphi\Big|_{1/2,k}^{n}. \quad (2.9)$$

If $m = 1$, $e_\varphi \neq 0$ and $h_\rho \neq 0$.

$$e_\varphi\Big|_{0,k+1/2}^{n+1/2} = e_\varphi\Big|_{0,k+1/2}^{n-1/2} - \frac{2\Delta t}{\varepsilon\Delta r} h_z\Big|_{1/2,k+1/2}^{n} + \frac{\Delta t}{\varepsilon\Delta z}\left(h_r\Big|_{0,k+1/2}^{n} - h_r\Big|_{0,k}^{n}\right),$$

$$h_\rho\Big|_{0,k}^{n+1} = h_\rho\Big|_{0,k}^{n} - \frac{\Delta t}{\mu\Delta r} e_z\Big|_{1,k}^{n+1/2} + \frac{\Delta t}{\mu\Delta z}\left(e_\varphi\Big|_{0,k+1/2}^{n+1/2} - e_\varphi\Big|_{0,k-1/2}^{n+1/2}\right). \quad (2.10)$$

The explicit finite-difference scheme described above becomes unstable with a certain choice of space and time step. The numerical limit of stability for the time step used in the BOR-FDTD algorithm can be empirically represented as $\Delta t \le \Delta x / sc$. Here Δx is a spatial step, $s \approx 1/(m+1)$ for $m > 0$, and $s = \sqrt{2}$ for $m = 0$ [89]. Thus, the renewal formulas (1.7) – (1.8) make it possible to calculate the values of the field components at the following moments of time through the values of the field components at previous moments of time.

In the described numerical scheme, some boundary conditions are used to limit the calculation domain. These conditions should model free space. For this purpose, conditions in the form of a perfectly matched layer (PML) were used [89]. Based on the technique proposed in [90], inside the PML layer

$$\begin{cases} rot\dot{\bar{H}} = j\omega\varepsilon\hat{\varepsilon}\dot{\bar{E}}, \\ rot\dot{\bar{E}} = -j\omega\mu\hat{\varepsilon}\dot{\bar{H}}. \end{cases} \tag{2.11}$$

Next, the construction of the PML for the *r*-direction is shown, for the z-direction, the PML is built similarly. Here, the following tensors of dielectric and magnetic permeability are introduced

$$\hat{\varepsilon} = \hat{\mu} = \hat{s} = \begin{bmatrix} S_\rho^{-1} S_\varphi S_z & 0 & 0 \\ 0 & S_\rho S_\varphi^{-1} S_z & 0 \\ 0 & 0 & S_\rho S_\varphi S_z^{-1} \end{bmatrix},$$

$$S_\rho = \kappa_\rho + \sigma_\rho / j\omega, \quad S_z = 1, \quad S_\varphi = \mathrm{K}_\varphi + \Sigma_\varphi / j\omega,$$

$$\mathrm{K}_\varphi = \left(\rho_0 + \int_{\rho_0}^{\rho} \kappa_\rho(\rho')\, d\rho'\right) / \rho, \quad \Sigma_\varphi = \left(\int_{\rho_0}^{\rho} \sigma_\rho(\rho')\, d\rho'\right) / \rho. \tag{2.12}$$

The value S_z is equal to one, which means there is no absorption in the *z* direction. The values κ_ρ and σ_ρ in (2.12) have the following dependence on the radial coordinate (here $r_{\max}$ is the maximum radial coordinate for PML, the parameters $\sigma_{\max}$, $\kappa_{\max}$ and a must change to obtain the minimum reflection)

$$\kappa_\rho(r) = 1 + \left[(r - r_1)/r_{\max} - r_1\right]^m \left(\kappa_{r,\max} - 1\right),$$
$$\sigma_r(r) = \sigma_{r,\max}\left[(r - r_1)/r_{\max} - r_1\right]^m,$$
$$\kappa_\varphi(r) = \int_{r_1}^{r} \kappa_r(r')\,dr' = (r - r_1)\left(\kappa_r(r) + m\right)/r(m+1) + r_1/r,$$
$$\sigma_\varphi(r) = \int_{r_1}^{r} \sigma_r(r')\,dr' = \sigma_r(r)(r - r_1)/r(m+1). \qquad (2.13)$$

As a result, the formulas for updating the field components inside the PML layer have the following form:

for calculation e_ρ

$$e_\rho\Big|_{i+1/2,k+1/2}^{n} = L_{i+1/2}^{\varphi}\, e_\rho\Big|_{i+1/2,k+1/2}^{n-1/2} - SLm_{i+1/2}^{\varphi}\, q_\rho\Big|_{i+1/2,k+1/2}^{n-1/2},$$
$$q_\rho\Big|_{i+1/2,k+1/2}^{n} = q_\rho\Big|_{i+1/2,k+1/2}^{n-1/2} - LSm_{i+1/2}^{r}\, d_\rho\Big|_{i+1/2,k+1/2}^{n-1/2},$$
$$d_\rho\Big|_{i+1/2,k+1/2}^{n+1/2} = d_\rho\Big|_{i+1/2,k+1/2}^{n-1/2} + \frac{\Delta t}{\varepsilon \Delta z}\left(h_\varphi\Big|_{i+1/2,k}^{n} - h_\varphi\Big|_{i+1/2,k+1}^{n}\right) -$$
$$- \frac{m\Delta t/\varepsilon}{(i+1/2)\Delta r} h_z\Big|_{i+1/2,k+1/2}^{n}, \qquad (2.14)$$
$$q_\rho\Big|_{i+1/2,k+1/2}^{n+1/2} = q_\rho\Big|_{i+1/2,k+1/2}^{n} + LSp_{i+1/2}^{r}\, d_\rho\Big|_{i+1/2,k+1/2}^{n+1/2},$$
$$e_\rho\Big|_{i+1/2,k+1/2}^{n+1/2} = e_\rho\Big|_{i+1/2,k+1/2}^{n} + SLp_{i+1/2}^{\varphi} p_{i+1/2}^{\varphi}\, q_\rho\Big|_{i+1/2,k+1/2}^{n+1/2},$$

for calculation e_φ

$$e_\varphi\Big|_{i,k+1/2}^{n} = e_\varphi\Big|_{i,k+1/2}^{n-1/2} - LSm_i^{\varphi}\, q_\varphi\Big|_{i,k+1/2}^{n-1/2},$$
$$q_\varphi\Big|_{i,k+1/2}^{n} = L_i^{r}\, q_\varphi\Big|_{i,k+1/2}^{n-1/2} - SLm_i^{r}\, d_\varphi\Big|_{i,k+1/2}^{n-1/2},$$
$$d_\varphi\Big|_{i,k+1/2}^{n+1/2} = d_\varphi\Big|_{i,k+1/2}^{n-1/2} + \frac{\Delta t}{\varepsilon \Delta r}\left(h_z\Big|_{i-1/2,k+1/2}^{n} - h_z\Big|_{i+1/2,k+1/2}^{n}\right) +$$

$$+\frac{\Delta t}{\varepsilon\Delta z}\left(h_\rho\Big|_{i,k+1}^{n}-h_\rho\Big|_{i,k}^{n}\right),$$

$$q_\varphi\Big|_{i,k+1/2}^{n+1/2}=q_\varphi\Big|_{i,k+1/2}^{n}+SLp_i^r\,d_\varphi\Big|_{i,k+1/2}^{n+1/2},\qquad(2.15)$$

$$e_\varphi\Big|_{i,k+1/2}^{n+1/2}=e_\varphi\Big|_{i,k+1/2}^{n}+LSp_i^\varphi\,q_\varphi\Big|_{i,k+1/2}^{n+1/2},$$

for calculation e_z

$$e_z\Big|_{i,k}^{n}=L_i^\varphi\,e_z\Big|_{i,k}^{n-1/2}-SLm_i^\varphi\,q_z\Big|_{i,k}^{n-1/2},$$

$$q_z\Big|_{i,k}^{n}=L_i^r\,q_z\Big|_{i,k}^{n-1/2}-SLm_i^r\,q_z\Big|_{i,k}^{n-1/2},$$

$$d_z\Big|_{i,k}^{n+1/2}=d_z\Big|_{i,k}^{n-1/2}+\frac{(i+1/2)\Delta t}{\varepsilon i\Delta r}h_\varphi\Big|_{i+1/2,k}^{n}-$$

$$-\frac{(i-1/2)\Delta t}{\varepsilon i\Delta r}h_\varphi\Big|_{i-1/2,k}^{n}+\frac{m\Delta t}{\varepsilon i\Delta r}h_r\Big|_{i,k}^{n},\qquad(2.16)$$

$$q_z\Big|_{i,k}^{n+1/2}=q_z\Big|_{i,k}^{n}+SLp_i^r\,d_z\Big|_{i,k}^{n+1/2},$$

$$e_z\Big|_{i,k}^{n+1/2}=e_z\Big|_{i,k}^{n}+SLp_i^\varphi\,q_z\Big|_{i,k}^{n+1/2},$$

for calculation h_ρ

$$h_\rho\Big|_{i,k}^{n+1/2}=L_i^\varphi\,h_\rho\Big|_{i,k}^{n}-SLm_i^\varphi\,a_\rho\Big|_{i,k}^{n},$$

$$a_\rho\Big|_{i,k}^{n+1/2}=a_\rho\Big|_{i,k}^{n}-LSm_i^r\,b_\rho\Big|_{i,k}^{n},$$

$$b_\rho\Big|_{i,k}^{n+1}=b_\rho\Big|_{i,k}^{n}+\frac{\Delta t}{\mu\Delta z}\left(e_\varphi\Big|_{i,k+1/2}^{n+1/2}-e_\varphi\Big|_{i,k-1/2}^{n+1/2}\right)-\frac{m\Delta t}{\mu i\Delta r}e_z\Big|_{i,k}^{n+1/2},$$

$$a_\rho\Big|_{i,k}^{n+1}=a_\rho\Big|_{i,k}^{n+1/2}+LSp_i^r\,b_\rho\Big|_{i,k}^{n+1},\qquad(2.17)$$

$$h_\rho\Big|_{i,k}^{n+1}=h_\rho\Big|_{i,k}^{n+1/2}+SLp_i^\varphi\,a_\rho\Big|_{i,k}^{n+1},$$

for calculation h_φ

$$
\begin{aligned}
&h_{\varphi}\Big|_{i+1/2,k}^{n+1/2} = h_{\varphi}\Big|_{i+1/2,k}^{n} - LSm_{i+1/2}^{\varphi}\, a_{\varphi}\Big|_{i+1/2,k}^{n},\\
&a_{\varphi}\Big|_{i+1/2,k}^{n+1/2} = L_{i+1/2}^{r}\, a_{\varphi}\Big|_{i+1/2,k}^{n} - SLm_{i+1/2}^{r}\, b_{\varphi}\Big|_{i+1/2,k}^{n},\\
&b_{\varphi}\Big|_{i+1/2,k}^{n+1} = b_{\varphi}\Big|_{i+1/2,k}^{n} + \frac{\Delta t}{\mu\Delta z}\left(e_z\Big|_{i+1,k}^{n+1/2} - e_z\Big|_{i,k}^{n+1/2}\right) +\\
&+\frac{\Delta t}{\mu\Delta z}\left(e_r\Big|_{i+1/2,k-1/2}^{n+1/2} - e_r\Big|_{i+1/2,k+1/2}^{n+1/2}\right),\\
&a_{\varphi}\Big|_{i+1/2,k}^{n+1} = a_{\varphi}\Big|_{i+1/2,k}^{n+1/2} + SLp_{i+1/2}^{r}\, b_{\varphi}\Big|_{i+1/2,k}^{n+1},\\
&h_{\varphi}\Big|_{i+1/2,k}^{n+1} = h_{\varphi}\Big|_{i+1/2,k}^{n+1/2} + LSp_{i+1/2}^{\varphi}\, a_{\varphi}\Big|_{i+1/2,k}^{n+1},
\end{aligned}
\tag{2.18}
$$

for calculation h_z

$$
\begin{aligned}
&h_z\Big|_{i+1/2,k+1/2}^{n+1/2} = L_{i+1/2}^{\varphi}\, h_z\Big|_{i+1/2,k+1/2}^{n} - SLm_{i+1/2}^{\varphi}\, a_z\Big|_{i+1/2,k+1/2}^{n},\\
&a_z\Big|_{i+1/2,k+1/2}^{n+1/2} = L_{i+1/2}^{r}\, a_z\Big|_{i+1/2,k+1/2}^{n} - SLm_{i+1/2}^{r}\, b_z\Big|_{i+1/2,k+1/2}^{n},\\
&b_z\Big|_{i+1/2,k+1/2}^{n+1} = b_z\Big|_{i+1/2,k+1/2}^{n} + \frac{i\Delta t}{\left(i+1/2\right)\mu\Delta r}e_{\varphi}\Big|_{i,k+1/2}^{n+1/2} -\\
&-\frac{\left(i+1\right)\Delta t}{\left(i+1/2\right)\mu\Delta r}e_{\varphi}\Big|_{i+1,k+1/2}^{n+1/2} + \frac{m\Delta t}{\left(i+1/2\right)\mu\Delta r}e_r\Big|_{i+1/2,k+1/2}^{n+1/2},\\
&a_z\Big|_{i+1/2,k+1/2}^{n+1} = a_z\Big|_{i+1/2,k+1/2}^{n+1/2} + SLp_{i+1/2}^{r}\, b_z\Big|_{i+1/2,k+1/2}^{n+1},\\
&h_z\Big|_{i+1/2,k+1/2}^{n+1} = h_z\Big|_{i+1/2,k+1/2}^{n+1/2} + SLp_{i+1/2}^{\varphi}\, a_z\Big|_{i+1/2,k+1/2}^{n+1}.
\end{aligned}
\tag{2.19}
$$

At the same time, the following coefficients, depending on the radial coordinate, are introduced

$$
\begin{aligned}
&L_i^{r,\varphi} = \left(2\kappa_i^{r,\varphi} - \sigma_i^{r,\varphi}\Delta t\right)\Big/\left(2\kappa_i^{r,\varphi} + \sigma_i^{r,\varphi}\Delta t\right),\\
&LSp_i^{r,\varphi} = \left(2\kappa_i^{r,\varphi} + \sigma_i^{r,\varphi}\Delta t\right)\Big/2, SLp_i^{r,\varphi} = \left(LSp_i^{r,\varphi}\right)^{-1},\\
&LSm_i^{r,\varphi} = \left(2\kappa_i^{r,\varphi} - \sigma_i^{r,\varphi}\Delta t\right)\Big/2, SLm_i^{r,\varphi} = \left(LSm_i^{r,\varphi}\right)^{-1}.
\end{aligned}
\tag{2.20}
$$

We use auxiliary variables $q_{\rho,\varphi,z}$, $d_{\rho,\varphi,z}$ (for electric field calculations) and $a_{\rho,\varphi,z}$, $b_{\rho,\varphi,z}$ (for magnetic field calculations) to calculate the field components in (2.14) – (2.19). It is important to note that in formulas (2.14) – (2.19) some field components are calculated outside the usual "leap-frog" time grid [89] (electric field components are calculated at integer points in time $e_\rho\big|^n, q_\rho\big|^n, e_\varphi\big|^n, q_\varphi\big|^n, e_z\big|^n, q_z\big|^n$, and the components of the magnetic field are calculated in half-integer points in time $h_r\big|^{n+1/2}, a_r\big|^{n+1/2}, h_\varphi\big|^{n+1/2}, a_\varphi\big|^{n+1/2}, h_z\big|^{n+1/2}, a_z\big|^{n+1/2}$.

These additional variables have only symbolic time indices. They are introduced for the convenience of calculations (when calculating using formula (2.14), only one variable is needed for the values $e_p\big|^{n-1/2}, e_p\big|^{n}, e_p\big|^{n+1/2}$, which are updated only in formula (2.14)) using expressions (2.14) – (2.19) and do not approximate the real values of the field at these moments of time.

The scheme of the computational PML region of a dielectric waveguide with an annular diaphragm is shown in Figure 2.1. Comparison of the field at a distance of one cell from the PML with the field at this point, calculated with a larger radial size of the computational domain, was carried out to check the influence of the PML domain on the computational scheme. From this study it was found that the error of the borders of the PML area is close to 0.15 %.

The field distribution corresponding to the spatial distribution of the mode under study (see formulas (2.1) – (2.4)) is created to excite the computational region in the transverse distribution of the waveguide to the diaphragm. The time dependence of the field is chosen in the form of a harmonic function with an appropriate frequency, which is smoothly turned on in order to reduce the impact of a sudden change of the field at $t = 0$ [90]. After that, the calculation of the field change in the studied structure is carried out until the steady-state mode is established. Values C_{mi} are calculated in cross-sections z_1 and z_2 before and after the grating to determine the reflection and transmission coefficients

$$C_{mi} = \int_0^{2\pi}\int_0^{a}\left(E_r\left(r,\varphi,z_i\right)E_r^{(m)}\left(r,\varphi\right) + E_\varphi\left(r,\varphi,z_i\right)E_\varphi^{(m)}\left(r,\varphi\right)\right)rdrd\varphi \,. \quad (2.21)$$

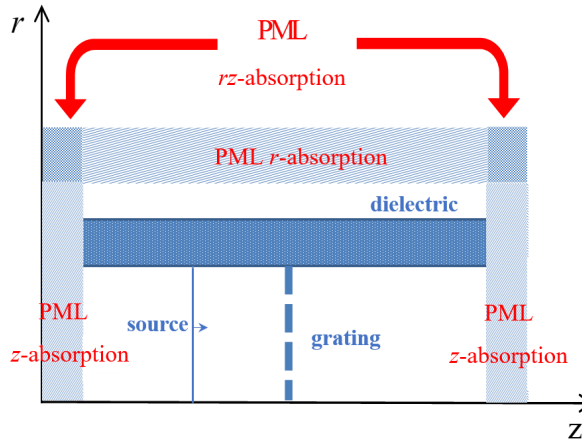

Figure 2.1. Scheme of the computational domain of a dielectric waveguide with a finite diaphragm

Here $E_r^{(m)}(r,\varphi)$ and $E_\varphi^{(m)}(r,\varphi)$ are the field distributions corresponding to the m-th mode (see formulas (2.1) – (2.3)). They are calculated using BOR-FDTD algorithm. If the mode with the number p is excited, then the reflection coefficient by power into this mode is equal to $(C_{p1}-1)^2$, and the reflection coefficients (transformation) into other modes are equal $(C_{p1}-1)^2$ (the incident wave has unit power). The transmission coefficient into this and other modes is calculated as $C_{ml}{}^2$.

For calculations of reflection coefficients of combined modes, it should be taken into account that the components of these modes (for example, TE_{0m} and EH_{1m} modes for $TE_{0m} + EH_{1m}$) diffract independently of each other on an axially symmetric diaphragm. First, a calculation is made for each of these modes separately, and then the reflection and transmission coefficients for the combined mode can be determined from the obtained results, taking into account the amplitude of each of the components.

The influence of the dielectric substrate on the scattering characteristics of the various modes should also be evaluated. In theoretical calculations, this part is not modeled in the FDTD scheme described above, because it leads to a significant increase in the time required to reach the stationary

mode due to a large number of reflections between the dielectric walls of the layer (preliminarily it can be estimated that this will lead to an increase in the calculation time by 5–10 times).

Thus, the following approach is used to model the substrate. Assume that the reflection and transmission coefficients for the substrate are equal to the reflection and transmission coefficients for the infinite layer. As it is known, the Fresnel power coefficients for a half-space with a refractive index n located in free space are equal to $R=(n-1)^2/(n+1)^2$, $T=4n/(n+1)^2$. The reflection and transmission coefficients for a layer of thickness L are equal

$$R_L = R + T^2 R\Delta/(1-R^2\Delta^2),\ T_L = T^2\Delta/(1-R^2\Delta^2),\ \Delta = e^{ikL}. \quad (2.22)$$

Here, the propagation constant k for the investigated mode in the waveguide is used in the phase multiplier. As a result, there are two inhomogeneities: the grating and the substrate. We denote the reflection and transmission coefficients for the grating obtained from the BOR-FDTD algorithm described above as R_g and T_g. Then the total reflection R_Σ and transmission coefficients T_Σ for the grating located on the dielectric substrate (on the dielectric layer) can be obtained taking into account the reflections between the grating and the layer in the following form

$$\begin{aligned} R_\Sigma &= R_g + T_g R_L T_g + T_g R_L R_g R_L T_g + T_g R_L R_g R_L R_g R_L T_g + \cdots, \\ T_\Sigma &= T_g T_L + T_g R_L R_g T_L + T_g R_L R_g R_L R_g T_L + \cdots. \end{aligned} \quad (2.23)$$

After simple transformations we get

$$R_\Sigma = R_g + T_g R_L T_g / \left[1-(R_L R_g)^2\right], T_\Sigma = T_g T_L / \left[1-(R_L R_g)^2\right]. \quad (2.24)$$

The presented algorithm for modeling the dielectric substrate was verified by comparison with the results of full FDTD simulation.

The described computational algorithm was tested in the article [91] for calculating the propagation of signals in a dielectric waveguide, as well as when solving the problem of scattering of electromagnetic waves on an azimuthally symmetrical metal small-scale diaphragm in a dielectric waveguide for a dielectric without losses [92], for a dielectric with losses [93]. The method for taking into account the dielectric substrate is described in [94].

2.1.2 An Inhomogeneous Mirror in a Quasi-optical Waveguide Resonator

The geometry of the investigated waveguide resonator, formed by an oversized dielectric waveguide of circular cross-section, closed on one end by a flat mirror, and on the other by a diffraction mirror in the form of an annular diaphragm, is shown in Figure 2.2.

The waveguide diameter (reflector aperture) with length L is denoted by $2a$. We will assume that the conditions of the quasi-optical approximation are fulfilled [95]: all dimensions of the resonator are larger than the wavelength λ ($L/\lambda >> 1$, $a/\lambda >> 1$), and the longitudinal dimensions are larger than the transverse ones ($L/a >> 1$). The dependence on time, proportional to $\exp(-i\omega t)$ ($\omega = ck$, c is the speed of light in a vacuum, $k = 2\pi/\lambda$), is further omitted.

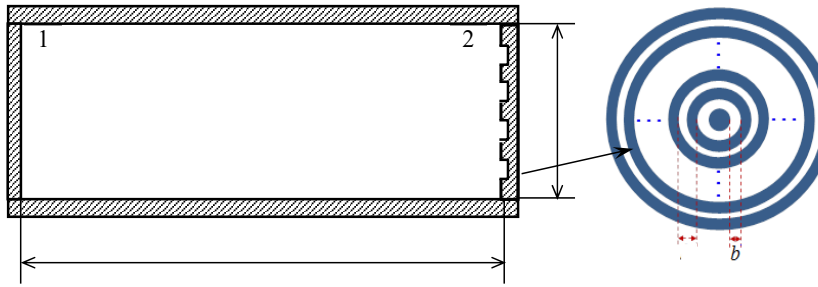

Figure 2.2. Scheme of a waveguide quasi-optical resonator: 1 – flat mirror; 2 – diffractive mirror

The theoretical approach to the calculation of waveguide resonators is based on the interpretation accepted for quasi-optical systems of the process of formation of types of oscillations as the interference of wave beams propagating towards each other, reflected by reflectors, as well as the display of the desired field distribution functions by the mode decomposition of the corresponding waveguide [96; 97]. Limiting ourselves to the axisymmetric case for mirrors, the interaction of oncoming beams with mirror *1* is described by the amplitude-phase correction function $\Phi_1(\rho) = 1$ ($\rho = r/a$ is the relative radial coordinate), and with mirror 2 by the amplitude-phase correction function $\Phi_2(\rho)$ proposed in [98] and it has the form:

$$\Phi_2(\rho)=\begin{cases}1, & Nl/a \le \rho \le Nl/a + d/a,\\ 0, & Nl/a\, l + d/a < \rho \le (N+1)\, l/a,\end{cases} \tag{2.25}$$

where $d = l - b$, l is the period of the nonuniform ring structure; b is the width of the dielectric ring on the period of the structure; N is the number of periods in the structure.

The complex amplitude of the field component of the wave beam propagating from mirror 1 to mirror 2 at the aperture of the latter is sought in the form

$$U(\rho,\varphi) = \sum_{m=1}^{M} C_m\, U_m^{(0)}(\rho,\varphi)\, e^{i\gamma_m L}, \tag{2.26}$$

where $U_m^{(0)}(\rho,\varphi)$ are the functions that characterize the modes of the hollow dielectric waveguide of the corresponding symmetry class; φ is the angular coordinate; λ are the propagation constants of waveguide modes of the corresponding class. The number M of terms in the expansion (2.26) is determined by the required accuracy of the calculation.

This component after the interaction of the wave with the reflector at its aperture can be represented by the following expression:

$$U(\rho,\varphi) = \sum_{m=1}^{M} C_m\, \Phi_2(\rho)\, U_m^{(0)}(\rho,\varphi)\, e^{i\gamma_m L}. \tag{2.27}$$

Let's rewrite (2.27), presenting $\Phi_2(\rho)U_m^{(0)}(\rho,\varphi)$ in the form of a series of eigen waveguide functions

$$U(\rho,\varphi) = \sum_{m=1}^{M} C_m \sum_{n=1}^{N} B_{2mn}\, U_n^{(0)}(\rho,\varphi)\, e^{i\gamma_n L}, \tag{2.28}$$

where $B_{2mn} = \int_0^1 \int_0^{2\pi} F_2(\rho) U_m^{(0)}(\rho,\varphi) U_n^{(0)}(\rho,\varphi) \rho\, d\rho\, d\varphi.$

Considering the complete round trip of the beam, describing its additional to the geometrooptical shift the phase shift and the amplitude reduction by the argument and the modulus of the number μ, as well as using the conditions of reproduction of the mode field per the round trip of the resonator [95], we obtain a system of equations for finding μ and C_m:

$$\mu C_k = e^{i\gamma_k L} \sum_{m=1}^{M} C_m \sum_{n=1}^{N} B_{2nk}\, e^{i\gamma_n L}, \quad k = 1,2,3,\ldots M. \tag{2.29}$$

Solving the system of linear algebraic equations (2.29) carried out using the modified LR-Rutishauser algorithm [98], which allows finding the eigenvalues of μ and the eigenvectors C_m, the components of which are the coefficients of the expansion of the resonator modes by waveguide waves. The relative fractions of energy of the waveguide waves forming the resonator mode are determined by the value

$$\chi_m = |C_m|^2 / \sum_{i=1}^{M} |C_i|^2 . \quad (2.30)$$

The complex eigenvalues determine the relative energy loss and additional to the geometrooptical shift the phase shift of the mode for the round trip of the resonator

$$\Delta_k = 1 - |\mu_k|^2 ; \ \Psi_k = \operatorname{Arg} \mu_k . \quad (2.31)$$

The relative intermode interval can be calculated using the formula

$$\Delta\nu_{kk'} = \frac{c}{2L}\left(\frac{\Psi_k - \Psi_{k'}}{2\pi}\right).$$

2.1.3. Calculation Results and Their Analysis

According to the method described above (subsection 2.1.2), the reflection and transmission coefficients of an axially symmetric diffraction grating located on a crystal quartz substrate were calculated for different modes of a hollow dielectric waveguide. As part of this method, the calculation domain, spatial resolution, and boundary conditions were specified. The step according to the spatial coordinates is chosen to be equal to $\Delta r = \Delta z = 10$ μm. Based on the technical conditions, the radius of the hollow dielectric glass waveguide was $a = 1750\Delta r = 17.5$ mm, the wall thickness of the waveguide was $t = 400\Delta r = 4$ mm. When calculating the field in glass, it is taken into account that its refractive index at the calculated wavelength ($\lambda = 432.6$ μm) is equal to $n = 2.57 + 0.15i$ [99]. The calculation area was set in size $1800\Delta r \times 80\Delta z$. In addition, marginal PML regions with a thickness of 15 cells are located on top and on both sides. The time step is chosen equal to $\Delta t = s\Delta z / c \approx 0.017$ ps (here c is the speed of light). The azimuthally symmetrical diffraction grating is located in the cross section $z_d = 50\Delta z$. It is a cylindrical grating of metal rings of width b with a given period l. The parameters of the inhomogeneous mirror were calculated using the BOR-FDTD numerical algorithm given above.

It made it possible to calculate the reflection and transmission coefficients of both symmetric and asymmetric waveguide modes with different field polarization through an axially symmetric diffraction mirror located inside a hollow circular dielectric waveguide. The calculations took into account the thickness of the quartz substrate, which was 3.1 mm. The studies were carried out at a wavelength of $\lambda = 432.6$ μm for diffraction mirrors with different periods l.

Calculations of the reflection coefficients R and transmittance T of TE_{01q}, TM_{01q} and EH_{11q} modes were performed for small-scale ($l < \lambda$), resonant ($l \approx \lambda$), and large-scale gratings ($l > \lambda$). Figure 2.3 provides graphs describing the dependences of the reflection and transmission coefficients of TE_{01q}, TM_{01q}, and EH_{11q} modes for gratings with a fixed filling factor $\eta = 0.5$. The periods of these diffraction gratings varied in the range from 120 μm to 1750 μm.

For the study of a small-scale mirror, when choosing the grating period, the conditions of the long-wave approximation $l << \lambda$ were fulfilled, and the results of this study are given in the papers [100; 103]. The period is chosen equal to l = 120 μm. Figure 2.4 presents the dependences of the reflection and transmittance coefficients of the grating on its filling factor η for TE_{01q}, TM_{01q} and EH_{11q} modes. The grating filling factor $\eta = b / l$ varied in the range 0 – 1. In order to excite a mode with the necessary spatially inhomogeneous polarization in the waveguide resonator of a THz laser, it is necessary that the mirror located at the exit of the resonator should provide a significant reflection of such modes ($R \geq 80$ %) and a significant transmission of modes with other undesirable types of polarization. As can be seen, the introduction into the waveguide of a mirror based on a small-scale multi-ring diaphragm with a filling factor of $\eta = 0.5$ leads to a significant increase in the reflection coefficients ($R > 90$ %) for the azimuthally polarized TE_{01q} oscillation type. This high reflection coefficient contributes to its generation in the laser. At the same time, this mirror provides fairly small reflection coefficients ($R \approx 30$ %) for linearly polarized EH_{11q} and radially polarized TM_{01q} modes.

For the study the resonant case, the period of the diffraction mirror was chosen to be close to the radiation wavelength ($l \approx \lambda$), and was l = 430 μm. Figure 2.5 presents the dependences of the reflection and transmission coefficients of this grating on its filling factor for TE_{01q}, TM_{01q} and EH_{11q}

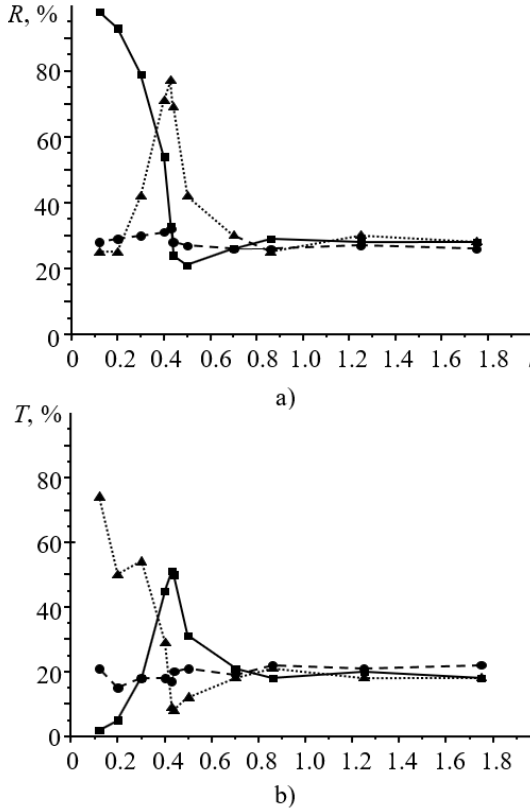

Figure 2.3. Dependencies of reflection *R* (a) and transmittance *T* (b) coefficients grating with a filling factor $\eta = 0.5$ from period *l* for modes TE_{01q} (solid line), TM_{01q} (dashed line) and EH_{11q} (dashed line)

modes. The filling factor of the grating varied in the range of 0 – 1. As can be seen, the introduction of a mirror with a resonant multi-ring diaphragm at $\eta = 0.5$ in the waveguide leads to a significant increase in the reflection coefficient ($R \geq 80$ %) for the radially polarized type of TM_{01q} oscillations, which contributes to its generation in the laser. At the same time, such a mirror provides fairly small reflection coefficients ($R \approx 30$ %) for linearly polarized EH_{11q} and azimuthally polarized TE_{01q} modes.

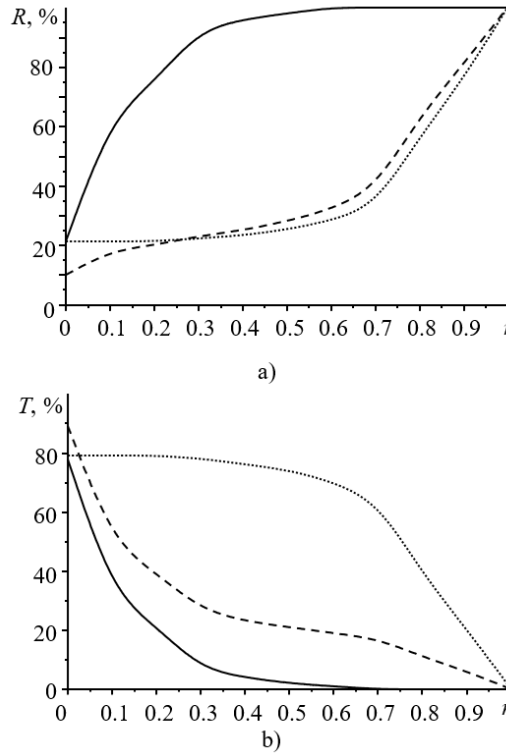

Figure 2.4. Dependencies of reflection *R* (a) and transmittance *T* (b) coefficients of a small-scale grating with a period of *l* = 120 μm from the filling factor *η* for modes TE_{01q} (solid line), TM_{01q} (dashed line) and EH_{11q} (dashed line)

Using a numerical algorithm, we also carried out numerical simulations of various large-scale diffraction mirrors, the period of which satisfies the condition $l > \lambda$. Using expressions (2.21 − 2.28), the relative energy losses per passage and phase shifts of the lower symmetric EH_{1mq}, TE_{0mq}, and TM_{0mq} modes of the investigated quasi-optical resonator, in which a diffraction grating in the form of an annular diaphragm was used as one of the mirrors, were calculated. The longitudinal index in the notation of resonator modes was omitted here. During the calculations, the length

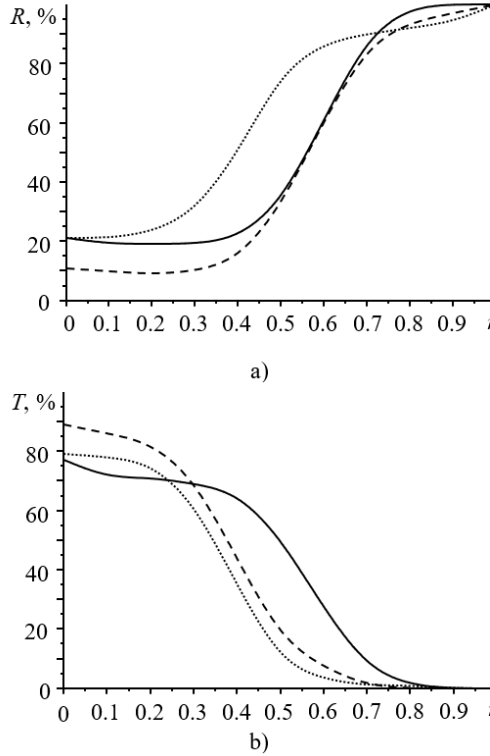

Figure 2.5. Dependencies of the reflection *R* (a) and transmittance *T* (b) coefficients of the resonant grating with a period of *l* = 430 μm on the filling factor *η* for modes TE_{01q} (solid line), TM_{01q} (dashed line), and EH_{11q} (dashed line)

of the glass waveguide (L = 565 mm) was chosen taking into account its further use in the WQR of the HCOOH laser (λ = 0.4326 mm). The calculation was carried out for a waveguide with a diameter of $2a$ = 25 mm. The number of waveguide modes m in each n-type of oscillations, which is determined by the required accuracy of the calculation, is chosen equal to m = 10. Crystalline quartz with a refractive index at the working wavelength n = 2.1073 and an absorption index k = 0.008 was chosen as the substrate material for the diffraction mirror [102]. Based on technological

capabilities and the need to ensure large-scale inhomogeneities, the period of the ring diffraction grating was chosen in the range l = (2.0÷3.5) λ. The size of the dielectric ring was d = 0.2 ÷ 0.6 mm. In the calculations, the reflection coefficient of radiation at the working wavelength from the quartz substrate of the diffraction mirror equal to R = 0.35 was taken into account.

The results of calculations of the total energy losses per pass δ, of the lower EH_{1mq}, TE_{0mq}, and TM_{0mq} modes for a quasi-optical resonator based on a glass waveguide at the period of the diffraction mirror l = 0.89 mm (~ 2 λ) are presented in Fig. 2.6, at l = 1.25 mm (~ 3 λ) – in Fig. 2.7 and l = 1.56 mm (~3.5 λ) – in Figure 2.8. As can be seen from Fig. 2.6, the relative energy loss during the passage of the azimuthally polarized TE_{01} mode in the resonator with a diffraction mirror period of the order of 2 λ is at least 18 %. Increasing the period of the diffraction mirror to 3 λ allows them to be reduced to 12 % (Figure 2.7). A further increase in the period of the diffraction mirror to 3.5 λ makes it possible to further reduce the loss of the investigated mode by 0.2 (Figure 2.8). However, in this case, the number of periods of the diffraction mirror becomes small – a/l = 8, which will not provide the necessary interference of wave beams reflected from the surface of the mirror. In this case, the investigated mirror loses its diffraction properties. At all values of the periods of the diffraction

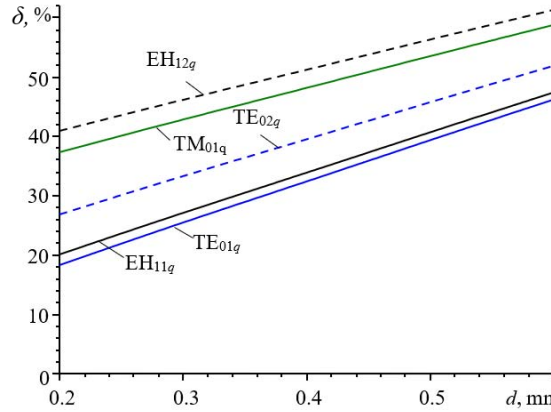

Figure 2.6. Dependences of the total energy loss per pass of the lowest-order modes of the resonator under study on the value of the dielectric diffraction ring of the mirror; l = 0.89 mm (2 λ)

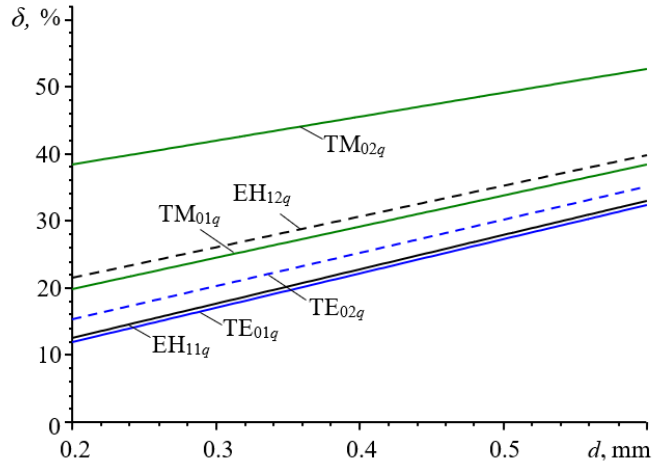

Figure 2.7. Dependences of the total energy loss per pass of the lowest-order modes of the resonator under study on the value of the dielectric diffraction ring of the mirror; l = 1.25 mm (3 λ)

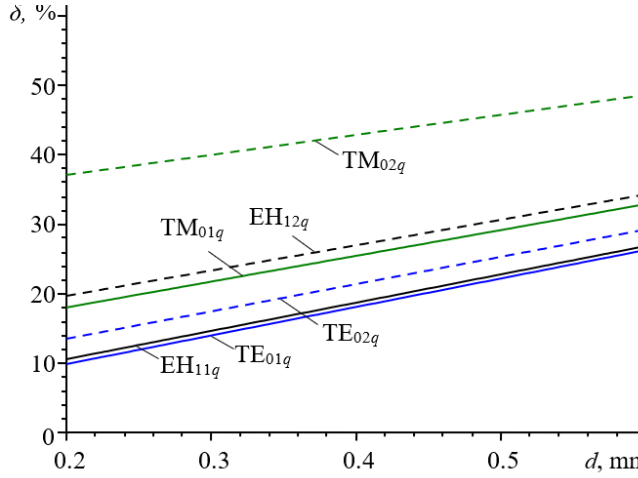

Figure 2.8. Dependences of the total energy loss per pass of the lowest-order modes of the resonator under study on the value of the dielectric diffraction ring of the mirror; l = 1.56 mm (3.5 λ)

mirror the dependence of the intermode intervals on the size of the dielectric ring remains constant. Figure 2.9 shows the dependences of the mode phase shifts of the resonator relative to the TE_{01q} mode. Modes TE_{01q} and TM_{01q} are degenerate in frequency.

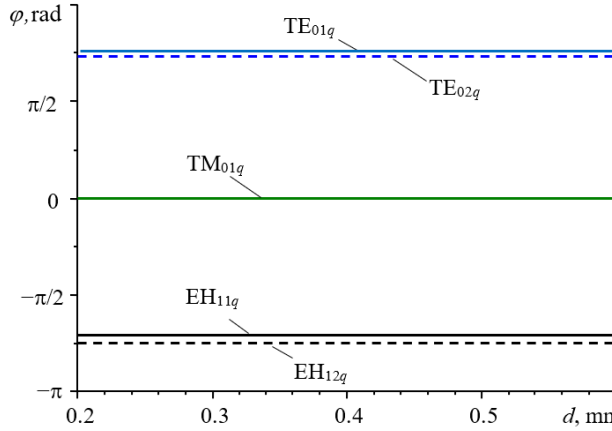

Figure 2.9. Dependences of the phase shifts of the resonator modes under study with respect to the TE_{01q} mode on the size of the diffractive dielectric ring of the mirror; l = 1.25 mm (3 λ)

2.2. EXPERIMENTAL SETUP

The structural diagram of a universal experimental setup based on a terahertz laser with optical pumping is shown in Figure 2.10.

The setup includes 5 main blocks:

– continuous dc-discharge CO_2 laser;

– a system of rotating mirrors, which ensures focusing of CO_2 laser radiation on the coupling hole of the mirror of the terahertz cell;

– terahertz cell;

– system of pumping and filling the terahertz cell with the working mixture;

– terahertz radiation registration system.

A continuous dc-discharge CO_2 laser is used in the setup to excite the working molecule of a terahertz laser. DC glow discharge is carried out from a stabilized source (*4*) with a voltage of 20 kV at a discharge current of

up to 40 mA. The laser resonator is formed by a spherical mirror (*7*) with a radius of curvature of 10 m and diffraction grating of the "echelette" type *8*. The length of the resonator is 1500 mm. By turning the grating the laser is retuned along the lines of generation of *P*- and *R*-branches. The echelette mirror (corner reflector) (*9*) is used to maintain the direction of the radiation coming out of the resonator into the zero order of the echelette. The laser works on a mixture of $CO_2 + N_2 + He + Xe$ gases in the ratio 1: 1: 4: 0.25 at the total pressure of the working mixture 12 mm Hg (1600 Pa).

The possibility of smooth tuning of the laser frequency within the contour of the amplification line is provided by moving the mirror (*7*). The mirror is fixed on a piezoelement of the KP-1 type, which provides a shift of ± 5 μm when a voltage of ± 50 V is applied to it from a direct current source (*5*). The laser radiation power at the centers *P* and *R* of the generation branches is at least 40 W. Laser radiation is modulated by a mechanical interrupter (*12*).

Figure 2.11 shows a record of the change in the output power of a quasi-soldered CO_2 laser from the moment of its powering and continuous operation during 5.5 hours. During this period of its operation, the capacity changed by no more than 10 %. This change is caused by temperature changes in the length of the resonator. A smooth decrease in power was not observed during the recording, which could be attributed to the degradation of the working mixture and a change in its total pressure.

A system of folding mirrors is formed by three flat mirrors (*11*) and a spherical mirror with a focal length of 0.5 m and provides the focusing of CO_2-laser radiation on a coupling hole of an input mirror (*14*) through the Brewster window of the terahertz cell. Such system for introducing pumping radiation into the cell provides a good separation of the CO_2 laser from the radiation reflected by the cell. This eliminates the influence of the terahertz cell during its frequency tuning on the CO_2 laser radiation characteristics.

The THz cell is a cylindrical vacuum chamber made from a segment of a circular hollow dielectric waveguide (*16*) with a diameter of 35 mm and a length of 1848 mm. A segment of the waveguide and two flat mirrors (*17, 18*) form a laser resonator. The input mirror (*17*) is copper with a central coupling hole of diameter 3 mm. Such inhomogeneity introduces insignificant changes in the losses and intensity distribution of the resonator modes. The output mirrors (*18*) are selected based on the need to obtain a given transverse generation mode, and they were either two-dimensional

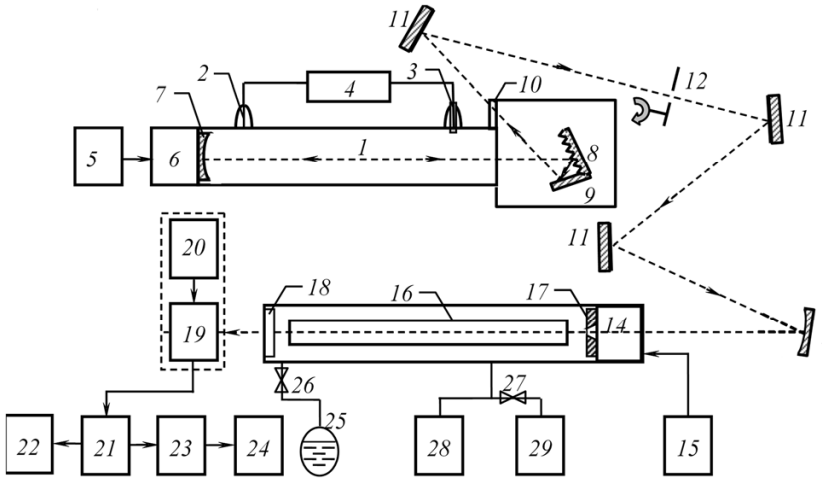

Figure 2.10. Structural diagram of the experimental setup: 1 – CO_2-laser; 2 – cathode; 3 – anode; 4 – high-voltage power source; 5 – constant voltage source; 6 – piezo element; 7, 13 – spherical mirrors; 8 – skeleton; 9 – corner reflector; 10 – NaCl plate; 11 – flat mirrors; 12 – mechanical modulator; 14 – mirror movement mechanism; 15 – electric drive; 16 – hollow dielectric waveguide; 17 – input mirror; 18 – output mirror; 19 – detector; 20 – beam scanning device; 21 – selective amplifier; 22 – oscilloscope; 23 – ADC; 24 – computer; 25 – flask with HCOOH; 26 – flow valve; 27 – shut-off valve; 28 – vacuum meter; 29 – vacuum pump

capacitive gratings or axially and radially symmetric diffraction gratings of various configurations. The input mirror (*17*) is fixed in the plane-parallel movement mechanism, which allows the mirror to be displaced by a distance of about 2 mm with a movement parallelism of at least 10'. Movement is carried out with the help of an electric motor.

The system for pumping out and filling the terahertz cell with the working mixture includes a fore-vacuum pump (*29*), a vacuum gauge (*28*), a shut-off valve (*27*), a leak valve (*26*), and a volume with working gas (*25*). This design of the injection system ensures a constant pressure of the working mixture in the terahertz chamber at the level of ~ 10^{-1} mm Hg (13 Pa).

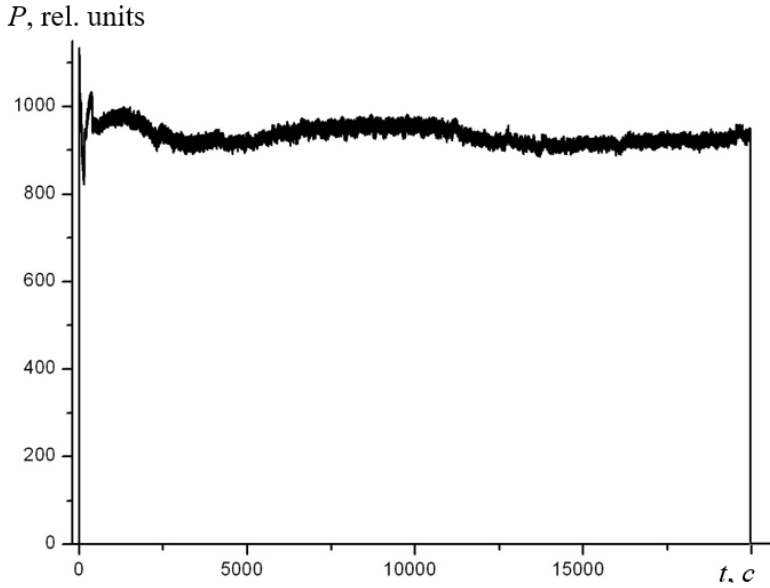

Figure 2.11. Change in the output power of a quasi-soldered tuning CO_2 laser during 5.5 hours of continuous operation (line 9P36)

The terahertz radiation registration system consists of a pyroelectric receiver (*19*) fixed in an electromechanical device, which allows scanning the transverse distribution of the laser radiation output intensity at different azimuths. The receiver could be located at distances from 10 cm to 1.5 m from the output mirror (*18*) of the cell.

The spatial resolution of the receiver was changed using diaphragms installed at its input. Volt-watt sensitivity and the expected width of the radiation beam were taken into account when choosing the resolution of the receiver. The diameter of the aperture was chosen in the range from 3 mm to 0.3 mm when measuring the spatial distribution of radiation intensity. The signal of the pyroelectric receiver was amplified by a selective amplifier (*21*) of the U2-8 type and fed to the ADC *23* and the computer (*24*). The signal of the amplifier was visually observed on an oscilloscope (*22)* of the C1-83 type.

The polarization state of the generated mode was determined as follows. The radiation receiver with a small input aperture was moved along different azimuths in the transverse plane of the radiation beam, and the position of the plane of polarization was determined at the points of maximum radiation using a polarizer. A one-dimensional wire grating with a step of 40 μm and a wire diameter of 8 μm was used as a polarizer.

The radiation power of the THz laser was determined by a BIMO-1 bolometric power transducer. The power of the CO_2 laser was measured by an IMO-2N calorimetric power meter. During the performance of the work the main experiments were conducted at a wavelength of 432.6 μm (generation line of a terahertz laser on a molecule of formic acid HCOOH, generation line of a CO_2 laser 9*R*20 with a wavelength of 9.27 μm).

The measurement technique is similar to that described in [101]. The spectrum of the natural modes of the resonator was recorded when the length of the resonator was changed by the electric drive *(15)*. The total energy losses σ during the round trip of resonator were determined by the measured width of the resonance curve. Transverse modes were identified by the intermode intervals, which were calculated from their phase shifts during a round trip of the resonator, and the transverse intensity distributions known from theory [88]. Measurement of the transverse intensity distributions near the output reflector of the resonator was carried out by scanning the pyroelectric receiver *(19)* with a spatial resolution of 1 mm across the direction of radiation propagation.

2.3. FORMATION OF LOWER-ORDER MODES WITH AZIMUTHAL POLARIZATION

2.3.1. Laser Resonator with a Large-scale Input and Homogeneous Output Mirrors

Using the technique described in subsection 2.1.2, calculations were made of the dependence of the reflection coefficient for waveguide resonator TE_{01q} and EH_{11q} modes with the lowest losses on the filling factor of an axially symmetric diffraction mirror located inside a hollow circular dielectric waveguide. In order to fulfil the condition of short-wavelength approximation $l > \lambda$ the grating period is chosen equal to $l = 1.75$ mm. Its filling factor $\eta = b/l$ varied in the range of 0.1 – 0.9. Calculations

showed that placing a mirror with a diffraction grating on the surface at $\eta > 0.8$ in the waveguide for the azimuthally polarized TE_{01q} type of oscillations makes it possible to obtain a reflection coefficient $R \geq 60$ %, and for the EH_{11q} mode with linear polarization – less than 50 % (Figure 2.12). This contributes to the selective excitation of the TE_{01q} mode in the laser cavity with the mirror under study.

In this case, a capacitive two-dimensional grating made by sputtering aluminum through a matrix onto a plane-parallel plate of crystalline quartz with a thickness of 4 mm was used as the initial homogeneous mirror of the resonator. An inductive tape grid with a period of 103 μm and a tape width of 17 μm was used as a matrix. Such a mirror has a transparency of 18 % at the working wavelength of the laser.

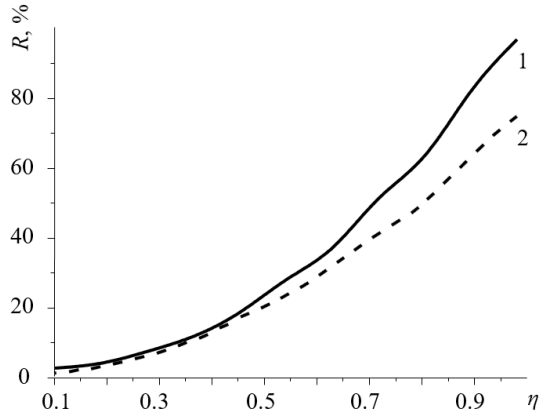

Figure 2.12. Dependences of the reflection coefficient R for TE_{01q} (1) and EH_{11q} (2) modes on the filling factor η of the multi-ring diaphragm

The input reflector was a inhomogeneous mirror with a central coupling hole with a diameter of $d = 3$ mm, the reflecting surface of which is proposed to be made in the form of an azimuthally symmetrical large-scale metal diffraction grating with a different quantity of reflecting rings and radiation-absorbing grooves of a width with a given period.

Taking into account the calculation results, the inhomogeneous input mirror was manufactured mechanically using a special cutter in the form

of nine reflective rings and radiation-absorbing grooves with a period l = 1.75 mm and a width of b = 0.35 mm. The profile of the reflector used in the experiment is shown in Fig. 2.13. Absorbing grooves were cut with a cutter to a depth of ~ 0.2 mm (~ 0.5 λ) at an angle of 30° to the plane of the reflecting surface of the mirror. This ensured that the rays from the laser resonator were removed from the surface of the grooves, which is similar to the almost complete absorption of radiation in these areas of the mirror.

Figure 2.14 shows the spectrum of excited modes of the laser obtained experimentally with the proposed input inhomogeneous mirror and output homogeneous capacitive mirror. Cavity length tuning reveals two cavity modes with the least losses. The second (by the Q-factor) mode has linear polarization and was identified as the EH_{11q} mode on the basis of its transverse field intensity distribution.

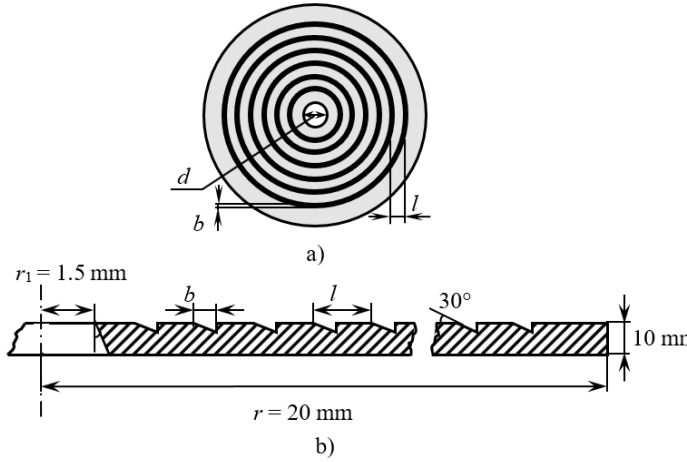

Figure 2.13. Profile of the input diffraction mirror: (a) relief of mirror surface and (b) transverse cross section of the mirror

The frequency distance between the EH_{11q} mode and the mode with highest Q-factor coincides with the theoretical calculations for the TE_{01q} mode. The transverse distribution of the field intensity of this mode in the far zone at the laser output is shown in Figure 2.15.

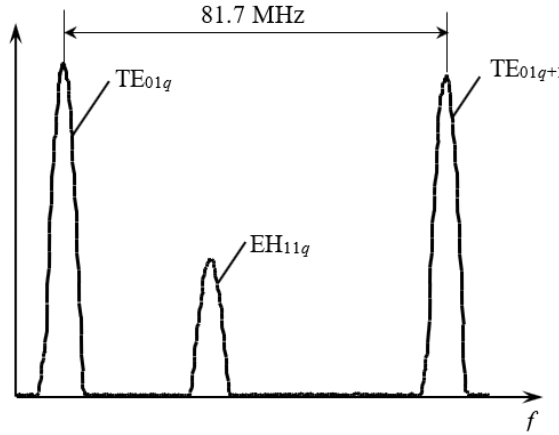

Figure 2.14. Tuning characteristic of a waveguide HCOOH laser with the input inhomogeneous mirror

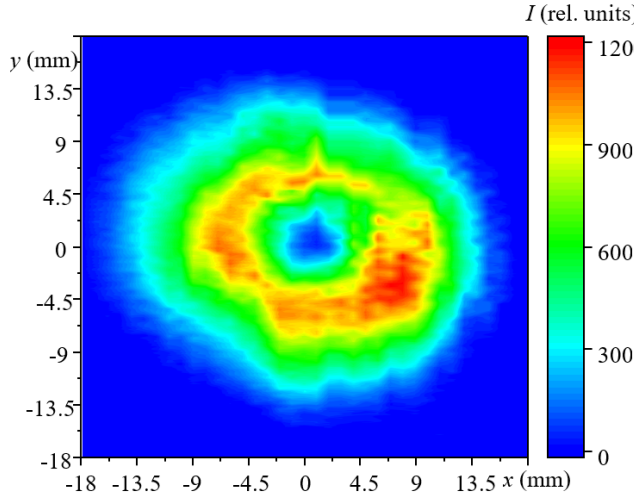

Figure 2.15. Experimental transverse distribution of radiation intensity *I* at the output of an HCOOH laser with an input large-scale mirror in the far zone for the TE_{01q} mode

Based on the transverse distribution obtained, the intermode distance in frequency, and the direction of the electric field vector for different azimuths, this mode is identified as the TE_{01q} mode with azimuthal polarization of radiation. The output power of the THz laser in the TE_{01q} mode was 8 mW, and in the EH_{11q} mode it was 3.75 mW. When the diffractive mirror was changed to a uniform laser radiation power in the EH_{11q} mode, it was 18 mW. The decrease in the radiation power in the EH_{11q} mode when using an inhomogeneous mirror is due to a decrease in the reflection coefficient of the mode from this mirror.

One can see that the proposed reflective azimuthally symmetrical large-scale diffraction mirror effectively selects undesired modes and can be simply realised in laboratory conditions. Nevertheless, because of its poor energy efficiency, further investigations were performed with small-scale diffraction structures arranged on the mirror surface.

2.3.2. Laser Resonator with Uniform Input and Small-scale Output Mirrors

A plane uniform aluminum mirror with a coupling hole with a diameter of 3 mm was at the entrance of the laser resonator as mirror *17* (Figure 2.10). Figure 2.16 shows the mirrors that were used as the output reflector *18*.

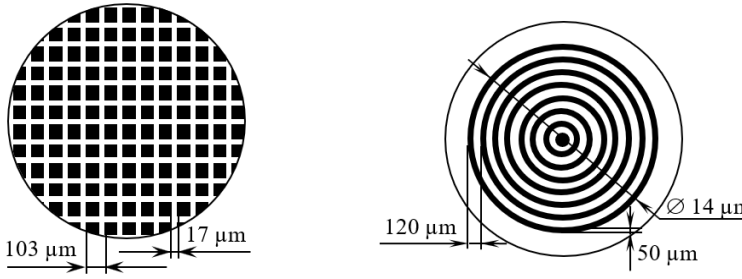

Figure 2.16. Output semitransparent mirrors of an optically pumped terahertz laser based on a capacitive grid and an azimuthally symmetric grating. I – two-dimensional capacitive grid; II – azimuthally symmetric diffraction grating without outer circles

Initially, a two-dimensional capacitive grid (Figure 2.16, mirror **I**) with a transparency of 20 % at a wavelength of 432.6 μm was used as the output mirror *18.* In this case, a characteristic type of the tuning characteristic is shown in Figure 2.17, which it is registered when the input mirror *17* is moved.

Five transverse modes were observed in the radiation spectrum. The transverse modes of laser generation are similar in terms of the field structure to the modes of a hollow dielectric waveguide. Their identification was carried out by comparing the measured experimental and calculated intermode distances for a dielectric waveguide resonator with the above parameters, according to degrees of polarization known from theory [50] and transverse intensity distributions of the observed modes.

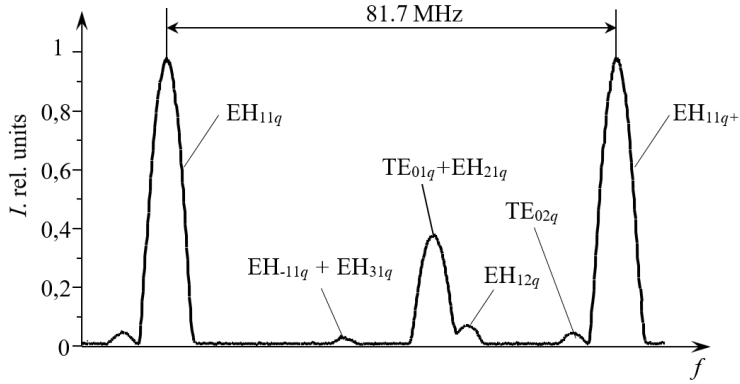

Figure 2.17. Mode spectrum of the HCOOH laser with an output uniform capacitive mirror

The experimentally measured and calculated transverse distributions of two modes with the maximum radiation power at a distance of 100 cm from the laser output mirror are shown in Figure 2.18. There is good agreement between experimentally measured and calculated data for radiation beams excited by EH_{11q}, $TE_{01q} + EH_{21q}$ modes.

Only one mode has a polarization other than linear from the two observed modes of generation. By comparing the calculated and measured intermode distances, it is identified as the TE_{02q} mode.

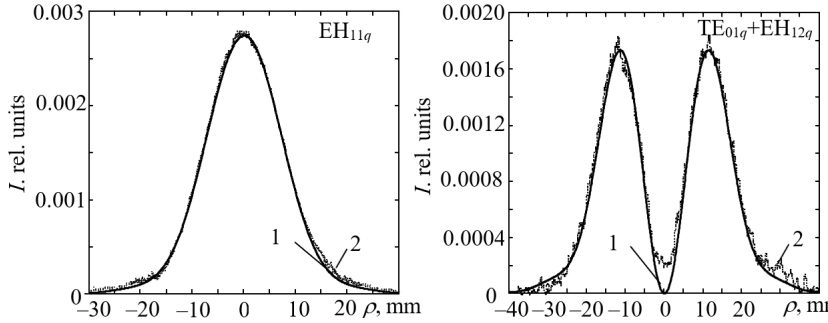

Figure 2.18. Calculated (1) and experimental (2) radial intensity distributions of the field for EH_{11q} and $TE_{01q}+EH_{21q}$ laser modes at a distance of 100 cm from the output mirror

Recently, a direction related to the use of diffraction mirrors with high polarization selectivity has been developing. The special pattern of their relief ensures the maximum *Q*-factor of the mode with the given direction of polarization [79]. In order to excite radiation with spatially inhomogeneous polarization in the waveguide resonator of a terahertz laser, it is necessary that the mirror located at the exit of the resonator provides greater reflection of such modes and significant transmission of modes with other undesirable types of polarization. For this purpose, it is proposed to use as the output mirror *18* an azimuthally symmetrical diffraction grating without outer rings, shown in Figure 2.16, mirror **II**. The azimuthally symmetrical diffraction grating was made by photolithography. A layer of aluminum with a thickness of 0.5 – 0.6 μm was applied to a plane-parallel plate of crystalline quartz with a thickness of 4 mm, in which areas of a given shape were etched. The grating period to fulfill the condition of long-wavelength approximation is chosen to be equal to 120 μm. The width of the reflective metallized circles is 50 μm, the grating filling factor is 0.4. Crystalline quartz at this wavelength has a low absorption index ($k = 0.008$) and a refractive index $n = 2.1$. When calculating the transparency of the mirror, the reflection from the crystalline quartz was not taken into account. So the measured and calculated values of the transmittance of the mirror differ. The measured reflection coefficient of the manufactured mirror at the wavelength of the pumping radiation is about 60 %.

The diameter of the diffraction grating on the mirror was d_0 = 14 mm. This configuration of the mirror is chosen based on the known transverse distributions of intensities for TE_{0n} modes and higher asymmetric waveguide modes. For symmetric TE_{0n} modes, which have a minimum field intensity in the center and on the periphery of the beam, mirror **II** also introduces minimal losses, which will increase with an increase in the mode index. The calculated reflection coefficient R of such a mirror for the TE_{01} waveguide mode was R – 50 %.

Figure 2.19 presents the tuning characteristics of the HCOOH laser with an output mirror based on an azimuthally symmetric diffraction grating without external circles. Their identification was carried out by comparing the measured and calculated intermode distances for the dielectric waveguide resonator with the above parameters, the degree of polarization of the output radiation, and the transverse intensity distributions of the observed modes of generation. The mode with the highest Q-factor was identified based on its transverse intensity distribution and radiation polarization state.

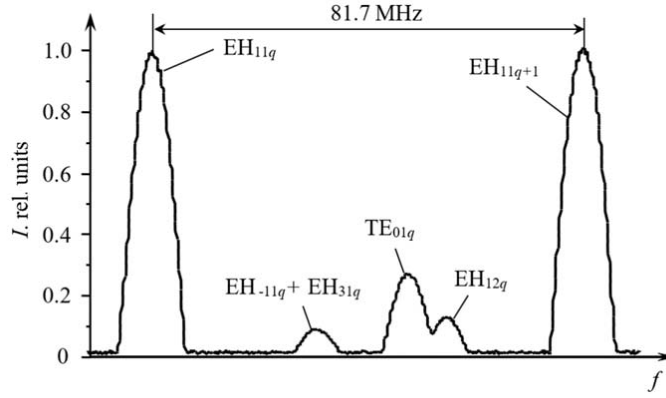

Figure 2.19. Mode spectrum of a waveguide HCOOH laser with an azimuthally symmetric diffraction mirror without outer circles

The mode with linear polarization of radiation, identified as the EH_{11q} mode, has the highest Q-factor. Modes with both linear and azimuthal polarization are also observed in the laser radiation spectrum. The second

most intense mode is identified as TE_{01} mode. For this confirmation research was conducted on the transverse distribution of the intensity of this mode (Figure 2.20). The position of the field strength vector *E* at different azimuths for this mode in the radiation intensity maxima is shown in Figure 2.21. A one-dimensional wire grating with a period of 40 μm and a wire diameter of 8 μm was used to determine the position of the vector *E*. As can be seen, the proposed initial azimuthal-symmetric small-scale diffraction mirror without outer circles selects undesired modes and

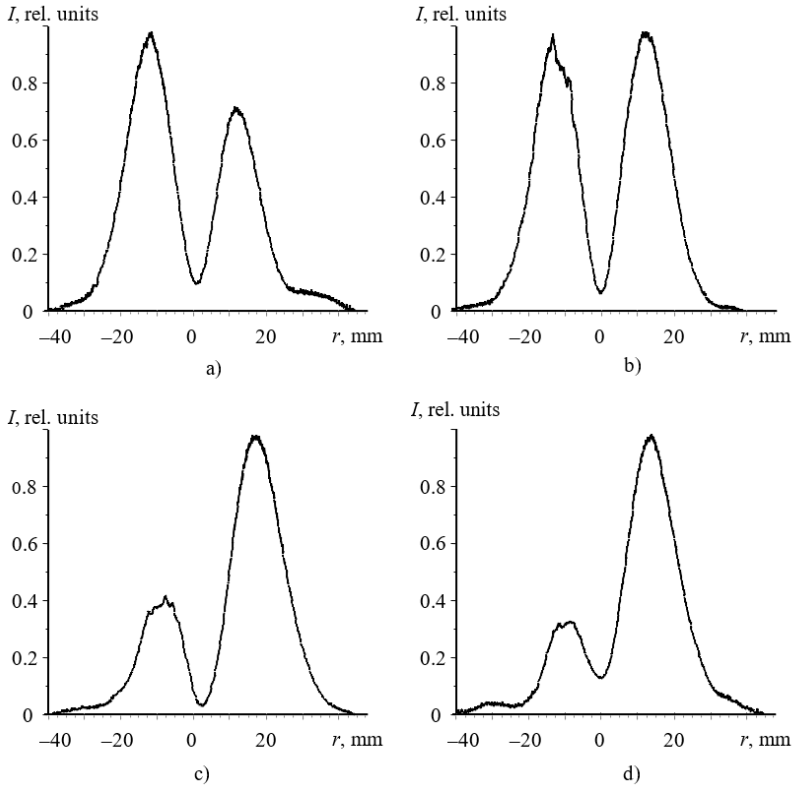

Figure 2.20. Transverse intensity distributions of the TE_{01q} mode at different azimuths: a) horizontal plane; b) 45°; c) vertical plane; d) 135°

forms the necessary mode with azimuthal polarization of radiation. However, it has a low energy efficiency compared to the well-known semitransparent small-scale diffractive mirror [100].

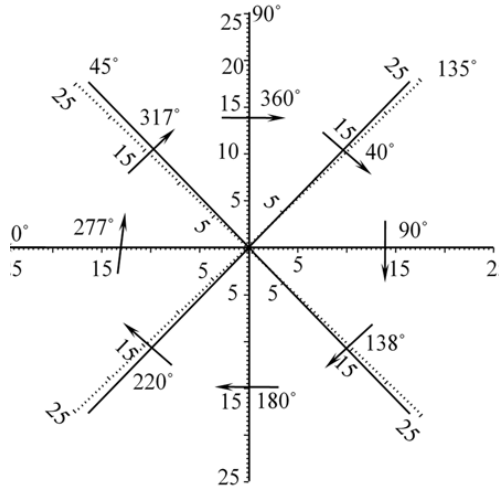

Figure 2.21. Position of the plane of polarization at the intensity maxima of the TE_{01q} mode at different azimuths. The direction of the electric field strength vector is chosen conditionally

2.4. FORMATION OF LOWER-ORDER MODES WITH RADIAL POLARIZATION

Figure 2.22 shows the mirrors as an output reflector (*18*) that were used to form modes with radial polarization. Radially symmetric diffraction gratings are made by the method of photolithography, which is described in the previous section. Three types of radially symmetric mirrors were fabricated for the experiments: sector-periodic mirror **I**, which has 628 aluminum-sputtered reflective sectors and the same number of uncoated nonreflecting sectors of equal angular width; mirror **II** with the same sector-periodic relief, but with an anti-reflective central region 12 mm in diameter; mirror **III** with the same sector-periodic relief, but with a well-reflecting central region 6.5 mm in diameter.

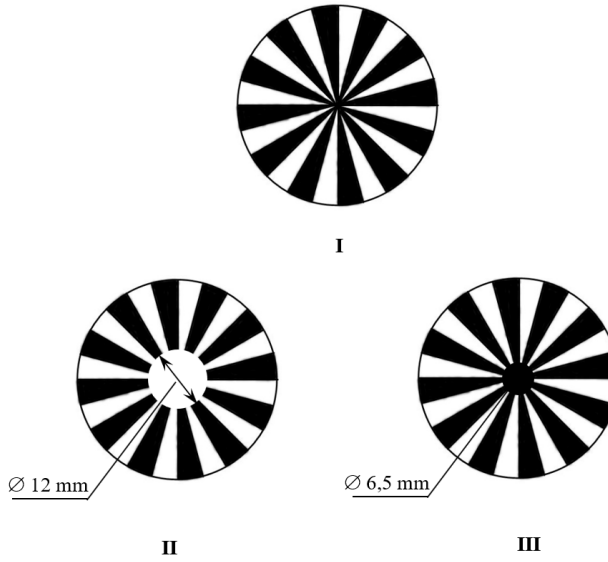

Figure 2.22. Output semitransparent mirrors based on radially symmetric gratings. I – radially symmetrical diffraction grating; II – radially symmetrical diffraction grating with an enlightened center; III – radially symmetrical diffraction grating with a center that reflects radiation

The tuning characteristic of the laser obtained using a radially symmetric diffraction grating **I** is shown in Figure 2.23. In this case five modes are observed. The higher intensity mode is identified as the EH_{11q} mode. Its transverse distribution in the horizontal and vertical planes at a distance of 70 cm from the output mirror is shown in Figure 2.24.

Other modes in this spectrum are identified by intermode distance and polarization as TM_{01q}, $TE_{01q}+EH_{21q}$ and EH_{12q} modes. However, the transverse distribution of these modes changes significantly. For example, the transverse distribution of the $TE_{01q}+EH_{21q}$ mode in the horizontal (a) and vertical (b) planes has the form presented in Figure 2.25. Its asymmetry is due to the fact that the TM_{01q}, $TE_{01q}+EH_{21q}$ and EH_{12q} modes have significant degeneracy.

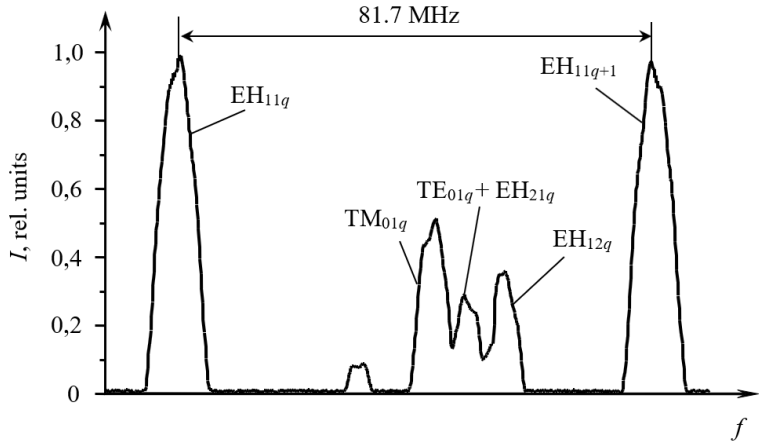

Figure 2.23. Mode spectrum of a waveguide HCOOH laser with a radially symmetric diffraction mirror

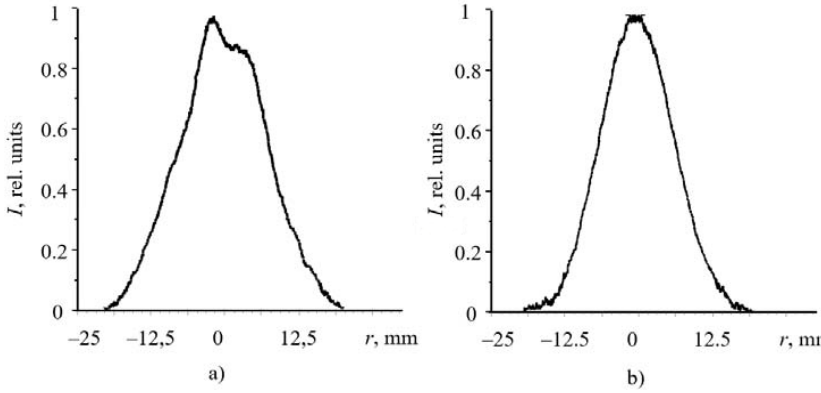

Figure 2.24. Transverse distribution of the EH_{11q} mode in the horizontal (a) and vertical (b) planes

Next, a radially symmetric grating with an illuminated central part with a diameter of 12 mm was investigated as the output mirror *18* of the terahertz cell (Figure 2.22, mirror **II**). The tuning characteristic of the laser, obtained by using a radial grating with an antireflective coating in the central part as

the output mirror (*18*) of the laser, is shown in Figure 2.26. Two modes of approximately equal intensity are observed in this characteristic. The radiation powers of the THz laser in these modes are 2.8 and 2.4 mW, respectively. Both modes have linear polarization.

The transverse distribution for higher intensity mode in the horizontal and vertical planes at a distance of 70 cm from the output mirror is shown

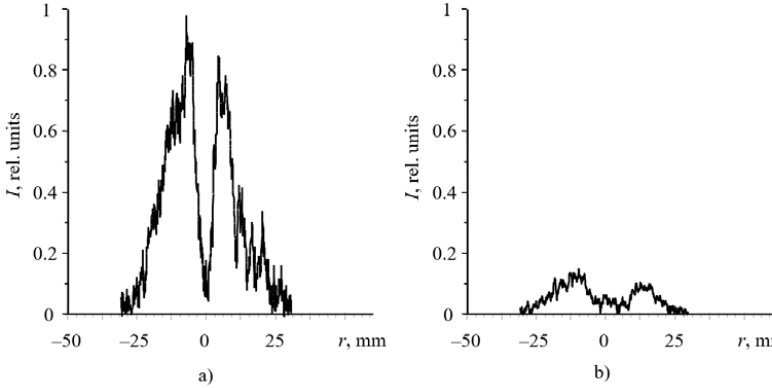

Figure 2.25. Transverse distribution of the TE_{01q}+EH_{21q} mode in the horizontal (a) and vertical (b) planes

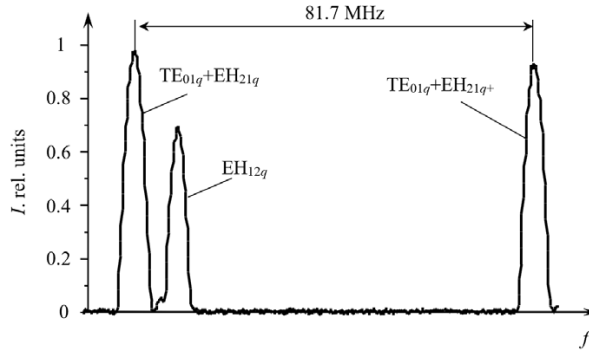

Figure 2.26. Mode spectrum of a waveguide HCOOH laser with a central part that reflects radiation in a radially symmetric diffraction mirror

in Figure 2.27. Considering these properties, as well as the intermode distance, it is identified as $TE_{01q}+EH_{21q}$ mode. The distribution of the second intensity mode in the horizontal and vertical planes at a distance of 70 cm from the output mirror is shown in Figure 2.28. The intermode distance and close to linear polarization allow us to identify this mode as EH_{12q} mode. The asymmetry in the transverse intensity distribution of this mode is associated with its frequency degeneracy with other modes.

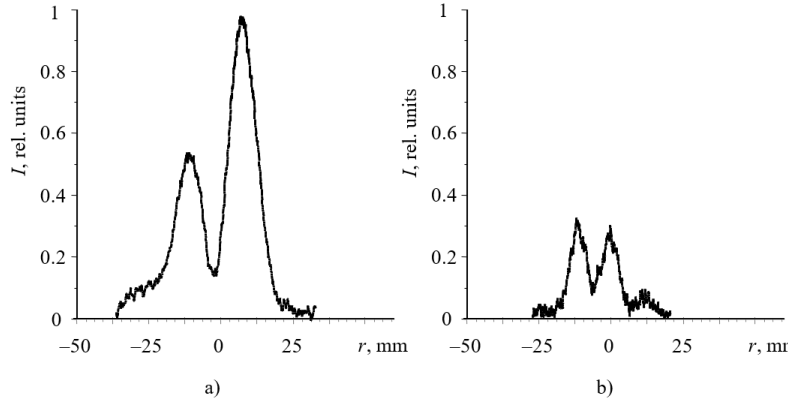

Figure 2.27. Transverse distribution of the $TE_{01q}+EH_{21q}$ mode in the horizontal (a) and vertical (b) planes

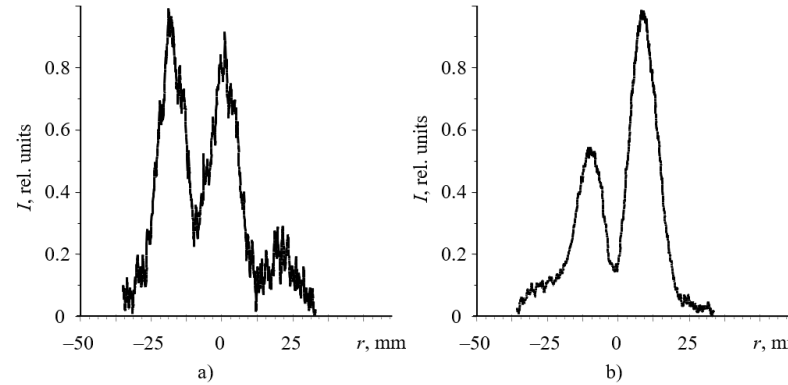

Figure 2.28. Transverse distribution of the EH_{12q} mode in the horizontal (a) and vertical (b) planes

Next, as the output mirror (*18*) of the terahertz cell, a radially symmetric grating with a center of 6.5 mm in diameter that reflects radiation was studied (mirror **III**, Figure 2.22). The tuning characteristic of the laser obtained with the use of this mirror is shown in Figure 2.29. We observe four modes in the spectrum. The transverse distribution of the basic mode in horizontal and vertical sections is shown in Figure 2.30. This mode has a linear polarization and we identified it as EH_{11q} mode. The second intensity mode has the transverse distribution which is shown in Figure 2.31.

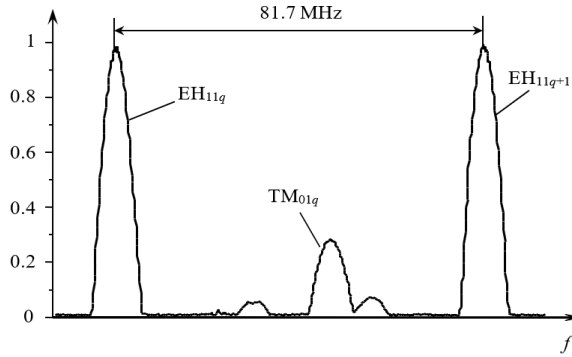

Figure 2.29. Mode spectrum of a waveguide HCOOH laser with a central part that reflects radiation in a radially symmetric diffractive mirror

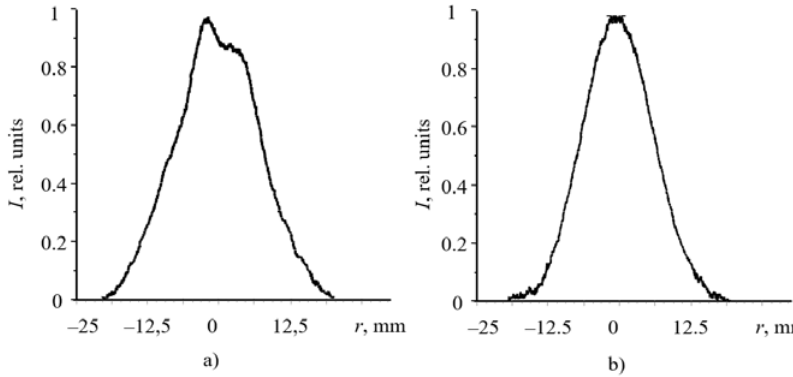

Figure 2.30. Transverse distribution of the EH_{11q} mode in the horizontal (a) and vertical (b) planes

The results of polarization measurements at the maxima of the radiation intensity distribution at different azimuths indicate that this mode has radial polarization (Figure 2.32). The transverse distribution profile, intermode distance and polarization type make it possible to identify it as TM_{01q} mode. Other mods have high losses, so they could not be identified.

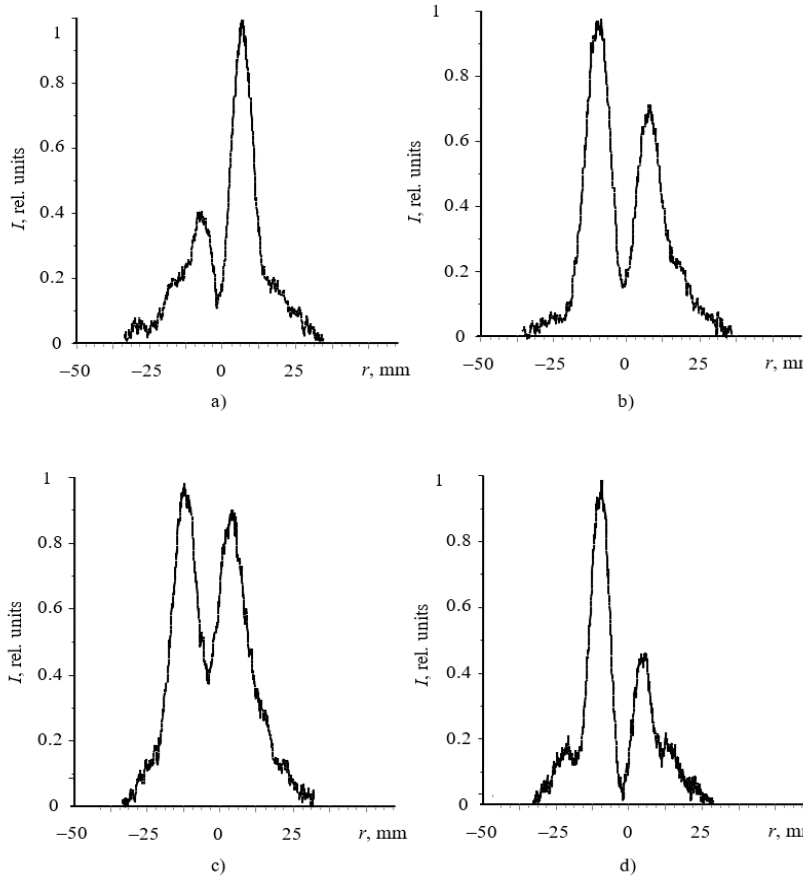

Figure 2.31. Transverse intensity distributions of the TM_{01q} mode at different azimuths. a) horizontal plane; b) 45°; c) vertical plane; d) 135°

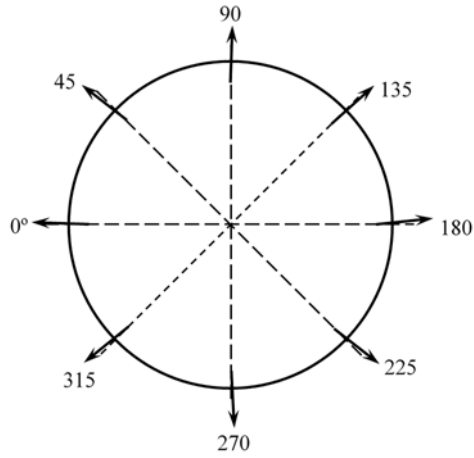

Figure 2.32 Position of the plane of polarization at the intensity maxima of the TM_{01q} mode at different azimuths. The direction of the electric field strength vector is chosen conditionally

Studies with radially symmetric mirrors of various configurations have shown that it is very difficult to select a mode with radial polarization. This could be done only by using a radially symmetric diffractive mirror **III** with a center that reflects radiation. The advantage of this mirror is that its structure with a reflective center has a negative effect on the modes that have a field maximum on the axis. Due to this, energy is transferred from the EH_{12q} mode to the required TM_{01q} mode.

2.5. FORMATION OF HIGHER-ORDER MODES WITH LINEAR POLARIZATION

Using the matrix technique described in subsection 2.1.2, calculations of the input phase-stepped mirror were carried out for the effective selection of the EH_{12q} mode in WQR with a high degree of discrimination of undesired modes. Figure 2.33 shows the calculated dependences of the total energy losses for the round trip of the modes of the investigated resonator on the width of the groove b of the diffraction mirror. It can be seen from the figure that by placing a groove with a width of $b = 1 – 1.2$ mm

(2.3 – 2.8) λ on the mirror, the losses for all undesired modes increase as much as possible, and the losses for the higher EH_{12q} mode remain practically unchanged.

For the formation of higher-order modes, a capacitive two-dimensional grid, made by sputtering aluminum through a matrix onto a plane-parallel plate of crystalline quartz with a thickness of 4 mm, was used as the initial homogeneous mirror of the resonator. The input reflector in this case was a homogeneous mirror with a central coupling hole with a diameter of d = 3 mm, the reflecting surface of which is proposed to be made with a groove with a width of b = 1.1 mm. Taking into account the results of the calculations, the nonuniform input phase-stepped mirror was done by a mechanical method using a special cutter. The profile of the reflector used in the experiment is shown in Figure 2.34. The absorbing groove was cut with a cutter to a depth of 0.11 mm ($\lambda / 4$) at a distance of 4.4 mm from the coupling hole. This ensured the selection of the higher EH_{12} mode in WQR with a high degree of discrimination of undesired modes.

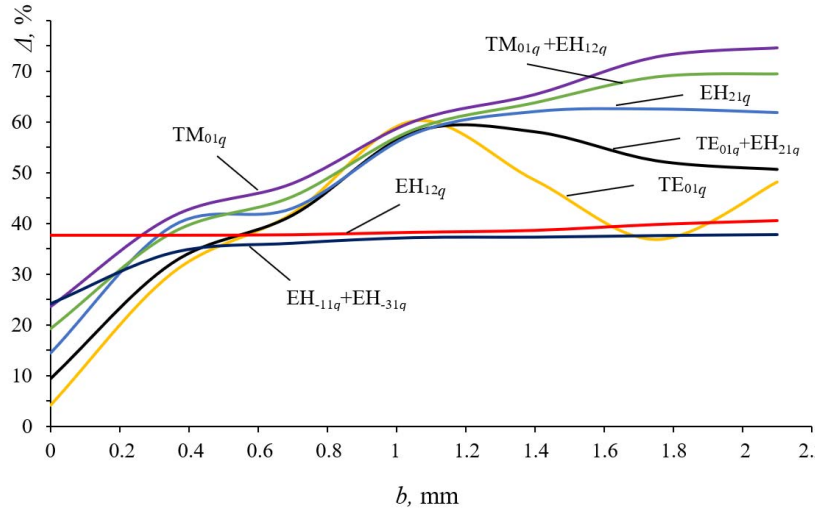

Figure 2.33. Calculated dependences of the total energy loss per round trip Δ

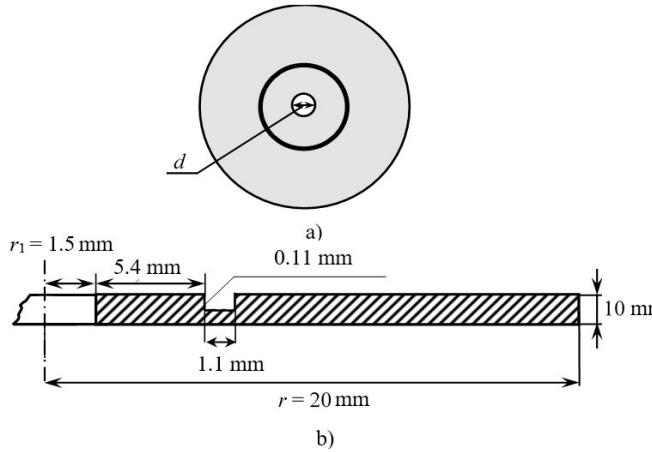

Figure 2.34. Profile of the input diffractive phase-stepped mirror: a) the relief of the surface of the mirror; b) cross section of the mirror

Figure 2.35 shows the spectrum of excited laser modes obtained experimentally using the proposed inhomogeneous input phase-stepped mirror and output uniform capacitive mirror. When the resonator length is tuned, 4 resonator modes are observed that have linear polarization and almost the same radiation power. The radiation power of the THz laser in the EH_{11q}, $TE_{01q}+EH_{21q}$ and $EH_{-11q}+EH_{31q}$ modes was 8 mW, and in the EH_{12q} mode it was 7.9 mW. These modes were identified on the basis of the obtained transverse distributions and intermode distances. The transverse distribution of the field intensity for the EH_{12q} mode in the far zone at the output of the laser is shown in Figure 2.36.

Thus, it is shown that the proposed phase-stepped mirror with a scattering groove effectively forms the required higher transverse mode with linear polarization.

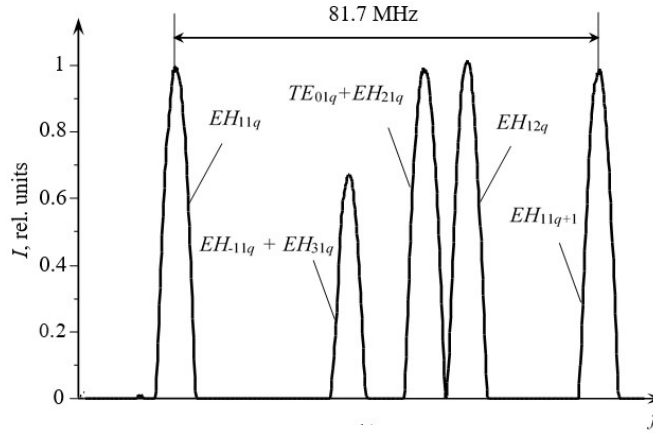

Figure 2.35. Mode spectrum of a waveguide HCOOH laser with an input phase-stepped mirror

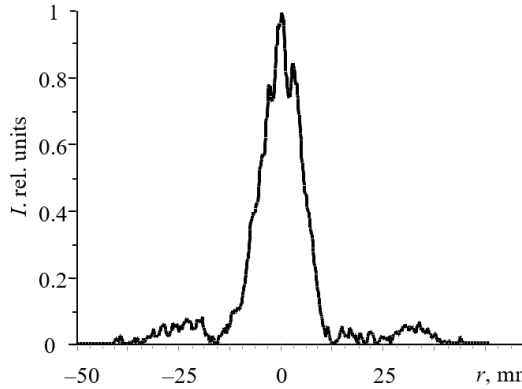

Figure 2.36. Experimental transverse distribution of radiation intensity *I* at a distance of 100 cm from the laser output mirror for the EH_{12q} mode

CHAPTER 3 «PROPAGATION OF THE TERAHERTZ LASER RADIATION WITH SPATIALLY INHOMOGENEOUS POLARIZATION IN DIFFERENT ZONES OF DIFFRACTION»

DOI: https://doi.org/10.30525/978-9934-26-461-0-3

The development of micro- and nanotechnologies requires new methods of formation and research of light fields with subwavelength dimensions of energy localization regions. Such problems are characterized by nonparaxial propagation of light and the impossibility of applying the scalar approximation. The distribution of electric field energy by components and, as a consequence, the polarization characteristics of radiation come to the fore.

Light beams are narrowly directed light radiation that spreads in a small body angle. If the beam divergence angle is small, $\theta \sim 10^{-3}$–10^{-2}, such a beam is called paraxial. In paraxial beams, the longitudinal component of the field is much smaller than the transverse components. Therefore, paraxial beams are usually described by one transverse component of the field. Such beams are called scalar. Most often, paraxial light beams are described as scalar, which is quite sufficient in most cases. Such a deliberately simplified approach is often used when describing the properties of light beams [104; 105]. However, for beams in which the divergence angle is large, the scalar approximation is not sufficient. Moreover, even for paraxial light beams, in which the polarization is nonuniform across the cross section, it is necessary to use a stricter vector formalism. Finally, the scalar approximation in all cases does not allow naturally describing the vector characteristics of the beam. It is more general to describe laser light beams as three-dimensional vector fields. However, vector beams have been studied much less (see, for example, [106]).

In [107], it was shown that when analyzing the diffraction of radiation beams, a zero value of the intensity on the optical axis is possible due to the presence of a longitudinal component of the field. Therefore, when studying the spatial-energy characteristics of laser beams, take into account the vector nature of the propagating radiation.

3.1. MODELING OF RADIATION PROPAGATION WITH INHOMOGENEOUS POLARIZATION IN DIFFERENT DIFFRACTION ZONES

In connection with the decrease in the size of laser systems, much attention has recently been paid to the description of nonparaxial propagation of light fields and the development of algorithms for modeling such propagation.

In [108], the propagation of a Gaussian beam in a homogeneous, isotropic, linear, and nonmagnetic dielectric medium was studied for the first time using the angular spectrum method. The electric field excited with a Gaussian beam in a dielectric medium is described by the expressions for the paraxial part and non-Gaussian correction terms of a higher order.

Characteristics for the propagation of azimuthally (or radially) polarized Lager-Gaussian beams for any optical systems described by the complex ABCD matrix were obtained [109]. These systems can have an arbitrary number of lenses, sections of free space and dielectrics, media with a radial amplification profile, spherical mirrors, reflectors. An analysis of the vector wave equation was carried out in [110]. A class of self-model solutions for the corresponding resonator modes with inhomogeneous polarization is derived. In [111] the solution of the Maxwell equations was proposed using the method of the plane wave spectrum of the electromagnetic field. In this representation, the solution of the electric field is written as the sum of two terms orthogonal to each other in the far zone. The concept of the near field to a given beam is introduced and applied to the known linearly polarized Gaussian beam.

In [112], the distribution of the field in the far zone, which is formed by the output ring modes with different polarization states, was studied using the Fresnel vector diffraction integral. It is shown that the azimuthal polarization is mainly transformed into radial during the propagation of ring beams with an azimuthal index above zero. This effect can contribute to increasing the productivity of a laser metal cutting system based on beams of this kind. In [113], the features of propagation in free space of light spirally polarized beams were studied in both paraxial and nonparaxial cases. Simple and important analytical results are obtained when the transverse intensity profile is chosen to correspond to a first-order axisymmetric Lager-Gaussian beam.

The polarization properties of vector coherent nonparaxial Gaussian beams are studied [114]. It is shown that when the radiation source of a nonparaxial Gaussian beam is fully polarized, the degree of polarization during field propagation maintains a constant value equal to unity. However, when the source is completely unpolarized, the degree of polarization during the propagation of the field does not keep a constant value, which is equal to zero. In [115], on the basis of the Rayleigh-Sommerfeld vector formula and using the relation between the Hermite and Lager polynomials, analytical expressions for the propagation of Hermite-Gaussian and Lager-Gaussian beams in the case of paraxial approximation are obtained with the corresponding expressions for propagation in the far zone, which are further derived for Gaussian beams as special cases of results. In [116], based on Rayleigh's vector diffraction integrals and the stationary phase method, an analytical expression was obtained that describes the propagation of the vector field of radially polarized Gaussian beams diffracted on an axicon.

The formula for the vector plane wave spectrum of an arbitrarily polarized electromagnetic wave in a homogeneous medium is derived using the method of mode decomposition of independent transverse fields [117]. This expression includes TM and TE modes for the spectrum of plane waves, where the amplitudes are separated and the polarization direction of each plane wave is given separately. In [118], based on the analysis of the vector structure of nonparaxial electromagnetic beams based on the stationary phase method, analytical expressions for the TE and TM modes of a linearly polarized Gaussian beam are presented in the nonparaxial approximation in the far zone. In [119], based on the Rayleigh-Sommerfeld vector formula, the nonparaxial propagation of radially polarized beams in free space was investigated analytically and with the help of numerical methods. An exact expression for describing the propagation of radially polarized light beams, which is valid for fields with an arbitrary transverse beam size, was obtained in a closed form for any point on the axis.

Based on the study of the vector structure of a electromagnetic beam and using the nonparaxial vector theory of moments, relations were presented for the beam radius, divergence angles and beam propagation factors in the nonparaxial case for a linearly polarized Gaussian beam and its TE and TM components [120]. In [121], a comparison of the results of calculations using the vector angular spectrum method and the Rayleigh-

Sommerfeld diffraction formula was made. On the basis of the angular spectrum method and the Weyl representation of a spherical wave, vector Rayleigh-Sommerfeld diffraction formulas of the first and second kind were obtained. In [122], analyzing the vector structure of an electromagnetic beam and using the stationary phase method, analytical expressions of the TE and TM components for a radially polarized Gaussian beam in the far zone were presented and a rigorous solution of Maxwell's equations was obtained for a confocal resonator. The components of the vector structure of the radially polarized Gaussian beam are compared with the components of the Gaussian TEM_{00} mode. Radially polarized "sophisticated" beams are considered in [123]. When describing such beams, the Lager polynomial has a complex argument, which is considered and analyzed. The features of the propagation of radially polarized beams in free space in the paraxial and nonparaxial cases are described from the point of view of the Rayleigh-Sommerfeld vector formula.

Using the vector angular spectrum method for an electromagnetic beam, the analytical vector structure of radially polarized beams is described [124]. The obtained results show that radially polarized beams consist only of TM waves. The concept of vector Lager-Bessel-Gaussian beams is proposed in [125]. On the basis of Rayleigh-Sommerfeld vector formulas, analytical formulas for the nonparaxial propagation of such vector beams were obtained [126] gives a description of a nonparaxial Gaussian beam based directly on Maxwell's equations. The vector angular spectrum method was used to solve these equations. Given the decomposition of the vector angular spectrum in the frequency domain into two terms, it is proposed to represent the nonparaxial Gaussian beam as the sum of two terms.

In [127], for a detailed description of the polarization features of nonparaxial radially polarized fields, a simple analytical propagation law using the method of the angular spectrum of plane waves is presented. Based on the parameter describing the width of the angular spectrum, a comparison was made between nonparaxial and paraxial results. In [128], using the angular spectrum method, general expressions were proposed to describe the propagation in free space of electromagnetic fields with a radial or azimuthal polarization structure in the transverse plane. The transverse distributions of the radial, azimuthal, and longitudinal components of these

fields were also analyzed. In particular, the features of the field on the axis during propagation in free space were studied.

Nonparaxial diffraction of Gaussian optical vortices with initial radial polarization was studied [129]. Explicit analytical expressions for the radial, azimuthal, and longitudinal components of the electric field intensity vector were obtained. Modeling showed that nonparaxial formulas describe the field much more accurately when moving away from the optical axis than paraxial ones. In [130], a general expression for the electric field of a cylindrically polarized vector beam propagating in free space was obtained on the basis of the exact vector solution of Maxwell's equations in the transverse Fourier plane. His analysis shows that the case of cylindrical polarization can be considered as a combination of radial and azimuthal polarizations and the electric field preserves cylindrical symmetry during propagation.

In [131], based on the method of the vector angular spectrum for electromagnetic beams and the method of the stationary phase, analytical vector formulas were obtained for describing the propagation of an annular beam in the far zone. Analytical expressions for finding the energy flow for TE- and TM-components and the entire annular beam in the far zone are presented. In [132], on the example of plane wave diffraction on a circular aperture in the near zone, a comparison of calculation algorithms using the vector integral Rayleigh-Sommerfeld transformation and expansion by plane waves was carried out in terms of accuracy and speed of calculations. A detailed analysis of the diffraction of a vortex beam at a circular aperture in the near zone was carried out using various calculation algorithms: vector integral Rayleigh-Sommerfeld transformation, expansion by plane waves, and the finite-difference time method [133]. Analytical expressions for the electromagnetic fields of radially polarized beams diffracted by a circular aperture are derived in [134] on the basis of Rayleigh's vector diffraction integral.

Analytical expressions for the electromagnetic fields of a cylindrically polarized vector beam propagating in free space were obtained in [135] on the basis of the vector angular spectrum and stationary phase methods. The analysis shows that azimuthal polarization in comparison with radial polarization is characterized by better energy focusing in the far zone. In [136], based on the angular spectrum method and the stationary phase

method, analytical expressions for studying the vector structure of a Gaussian beam diffracted at an aperture in the far zone were obtained in a rigorous form. In [137], based on the vector angular representation of the beam spectrum and the stationary phase method, an analytical expression for a cylindrically polarized Lager-Gaussian beam diffracted by a circular aperture in the far zone was obtained. The contribution of propagating waves and evanescent waves associated with nonparaxial light fields that propagate freely and in which the transverse component of the field is azimuthally polarized in an arbitrary plane was studied [138]. The analysis is carried out within the framework of the approach of the angular spectrum of plane waves. In [139], four fast and rigorous methods for modeling light propagation in a homogeneous medium are presented. It is shown that when studying the propagation of radiation beams in free space, analytical processing of rapidly oscillating phase components is very effective in reducing computational costs.

This section describes theoretical and experimental studies of the features of the structure of the field of laser radiation beams excited by the modes of the waveguide circular resonator of a THz laser in free space in diffraction zones with different types of spatial polarization of these modes.

3.2. PROPAGATION OF RADIATION OF TERAHERTZ LASER BASED ON A METALLIC CIRCULAR WAVEGUIDE IN DIFFERENT DIFFRACTION ZONES

3.2.1. Theoretical Relations

The propagation of laser radiation in free space along the 0z axis will be described by the well-known Rayleigh–Sommerfeld integrals [140]:

$$E_x(\vec{r}) = -\frac{1}{2\pi}\iint_{\Sigma_0} E_x^0(\vec{r}_0)\frac{\partial}{\partial z}\left[\frac{\exp(ikR)}{R}\right]dx_0dy_0,$$

$$E_y(\vec{r}) = -\frac{1}{2\pi}\iint_{\Sigma_0} E_y^0(\vec{r}_0)\frac{\partial}{\partial z}\left[\frac{\exp(ikR)}{R}\right]dx_0dy_0, \qquad (3.1)$$

$$E_z(\vec{r}) = \frac{1}{2\pi}\iint_{\Sigma_0} E_x^0(\vec{r}_0)\frac{\partial}{\partial x}\left[\frac{\exp(ikR)}{R}\right]dx_0dy_0 + \frac{1}{2\pi}\iint_{\Sigma_0} E_y^0(\vec{r}_0)\frac{\partial}{\partial y}\left[\frac{\exp(ikR)}{R}\right]dx_0dy_0,$$

where $E_x^0(\vec{r}_0)$ and $E_y^0(\vec{r}_0)$ are the complex amplitudes of the x and y components of the input electric field is given, the z-component is assumed to be zero due to the choice of the coordinate system, $\sum_0$ is the area in which the input field is specified, $k = 2\pi/\lambda$ is the wave number, λ is the wavelength $\vec{r}_0 = x_0\vec{e}_{x_0} + y_0\vec{e}_{y_0}$, (x_0, y_0) are the Cartesian coordinates in the input plane, $\vec{r} = x\vec{e}_x + y\vec{e}_y + z\vec{e}_z$, (x, y, z) are the Cartesian coordinates in the observation plane, $R = \sqrt{(x-x_0)^2 + (y-y_0)^2 + z^2}$. Using the nonparaxial approximation (3.1), we expand R into a series, keeping its first and second terms in the form

$$R \cong r + \frac{x_0^2 + y_0^2 - 2xx_0 - 2yy_0}{2r}. \tag{3.2}$$

Substituting (3.2) into the rapidly oscillating integrals and into other places $R \cong r$, and passing to cylindrical coordinates, we obtain expressions for the field components in different diffraction zones:

$$\begin{aligned}
E_x(\vec{r}) &= \frac{-z(ikr-1)}{2\pi r^3} e^{ikr} \times \\
&\times \int_0^{2\pi}\int_0^{\infty} E_x^0(\vec{r}_0)\cdot \exp\left(\frac{ik\rho_0^2}{2r}\right)\cdot \exp\left(-ik\frac{\rho\rho_0 cos(\varphi-\beta)}{r}\right)\rho_0 d\rho_0 d\varphi, \\
E_y(\vec{r}) &= \frac{-z(ikr-1)}{2\pi r^3} e^{ikr} \times \\
&\times \int_0^{2\pi}\int_0^{\infty} E_y^0(\vec{r}_0)\cdot \exp\left(\frac{ik\rho_0^2}{2r}\right)\cdot \exp\left(-ik\frac{\rho\rho_0 cos(\varphi-\beta)}{r}\right)\rho_0 d\rho_0 d\varphi, \\
E_z(\vec{r}) &= \frac{(ikr-1)}{2\pi r^3}\cdot e^{ikr} \times \\
&\times \int_0^{2\pi}\int_0^{\infty}\left[E_x^0(\vec{r}_0)(\rho\cos\beta - \rho_0\cos\varphi) + E_y^0(\vec{r}_0)(\rho\sin\beta - \rho_0\sin\varphi)\right]\times \\
&\times \exp\left(\frac{ik\rho_0^2}{2r}\right)\cdot \exp\left[-ik\frac{\rho\rho_0\cos(\varphi-\beta)}{r}\right]\rho_0 d\rho_0 d\varphi.
\end{aligned} \tag{3.3}$$

Here (ρ, β, z) are cylindrical coordinates in the observation plane and (ρ_0, φ) are polar coordinates in the region of the input field setting. In this case $R \approx r + \frac{\rho_0^2 - 2\rho\rho_0\cos(\varphi-\beta)}{2r}$.

The modes of the studied laser resonator coincide with the modes of a circular hollow dielectric waveguide. Let the given radiation in the initial plane be in the form of azimuthally symmetric TE_{0n} modes of a circular metal waveguide, the field components of which in the source plane $z = 0$ have the form:

$$E_x^0\left(\vec{r_0},0\right) = -A_{0n}J_1\left(\frac{\chi'_{0n}\rho_0}{a}\right)\sin\varphi,$$
$$E_y^0\left(\vec{r_0},0\right) = A_{0n}J_1\left(\frac{\chi'_{0n}\rho_0}{a}\right)\cos\varphi, \tag{3.4}$$

where $A_{0n} = \dfrac{1}{\left(J_0(\chi'_{0n})\sqrt{\pi}\right)a}$ is the normalizing factor, χ'_{0n} the nth root of the equation $J'_0(\chi') = 0$. Using expression (3.3) and the reference integral $\int\limits_0^{2\pi}\begin{Bmatrix}\cos(m\phi)\\ \sin(m\phi)\end{Bmatrix}\exp\left[-ix\cos(\phi-\theta)\right]d\phi = 2\pi(-i)^m J_m(x)\begin{Bmatrix}\cos(m\phi)\\ \sin(m\phi)\end{Bmatrix}$, we obtain expressions for the field components in different diffraction zones:

$$\begin{cases} E_x\left(\vec{r}\right) = -\dfrac{iz(ikr-1)}{r^3}e^{ikr}\times \\ \qquad\qquad \times A_{0n}\sin\beta\int_0^a J_1\left(\dfrac{\chi'_{0n}\rho_0}{a}\right)e^{ik\frac{\rho_0^2}{2r}}J_1\left(\dfrac{k\rho_0\rho}{r}\right)\rho_0 d\rho_0, \\ E_y\left(\vec{r}\right) = \dfrac{iz(ikr-1)}{r^3}e^{ikr}\times \\ \qquad\qquad \times A_{0n}\cos\beta\int_0^a J_1\left(\dfrac{\chi'_{0n}\rho_0}{a}\right)e^{ik\frac{\rho_0^2}{2r}}J_1\left(\dfrac{k\rho_0\rho}{r}\right)\rho_0 d\rho_0, \\ E_z\left(\vec{r}\right) = 0. \end{cases} \tag{3.5}$$

Next, we consider radiation in the initial plane in the form of radially symmetric TM_{0n} modes, whose field in the form of a source $z = 0$ has the form:

$$\begin{cases} E_x^0\left(\vec{r_0},0\right) = A_{0n}J_1\left(\dfrac{\chi_{0n}\rho_0}{a}\right)\cos\varphi, \\ E_y^0\left(\vec{r_0},0\right) = A_{0n}J_1\left(\dfrac{\chi_{0n}\rho_0}{a}\right)\sin\varphi, \end{cases} \tag{3.6}$$

where $A_{0n} = 1\Big/\left(J_1\left(\chi'_{0n}\right)\sqrt{\pi}\right)a$ is the normalizing factor, χ_{0n} is the nth root of the equation $J_0(\chi_{0n}) = 0$. Then, using expression (3.3) and the above reference integral, we obtain expressions for the components of the field of these modes in the diffraction zones:

$$\begin{cases} E_x\left(\vec{r}\right) = \dfrac{iz(ikr-1)}{r^3}e^{ikr}A_{0n}\cos\beta\times \\ \qquad \times\int_0^a J_1\left(\dfrac{\chi_{0n}\rho_0}{a}\right)e^{ik\frac{\rho_0^2}{2r}}J_1\left(\dfrac{k\rho_0\rho}{r}\right)\rho_0 d\rho_0, \\ E_y\left(\vec{r}\right) = \dfrac{iz(ikr-1)}{r^3}e^{ikr}A_{0n}\sin\beta\times \\ \qquad \times\int_0^a J_1\left(\dfrac{\chi_{0n}\rho_0}{a}\right)e^{ik\frac{\rho_0^2}{2r}}J_1\left(\dfrac{k\rho_0\rho}{r}\right)\rho_0 d\rho_0, \\ E_z\left(\vec{r}\right) = \dfrac{(ikr-1)}{r^3}e^{ikr}A_{0n}\times \\ \qquad \int_0^a J_1\left(\dfrac{\chi_{0n}\rho_0}{a}\right)e^{ik\frac{\rho_0^2}{2r}}\left[-i\rho J_1\left(\dfrac{k\rho_0\rho}{r}\right)-\rho_0 J_0\left(\dfrac{k\rho_0\rho}{r}\right)\right]\rho_0 d\rho_0. \end{cases} \tag{3.7}$$

We also consider radiation in the initial plane in the form of asymmetric TE_{1n} modes, the field of which in the source plane $z = 0$ has the form:

$$\begin{cases} E_x^0 = A_{1n}J_2\left(\dfrac{\chi_{1n}\rho_0}{a}\right)\sin 2\varphi, \\ E_y^0 = A_{1n}\left[J_0\left(\dfrac{\chi_{1n}\rho_0}{a}\right)-J_2\left(\dfrac{\chi_{1n}\rho_0}{a}\right)\right]\cos 2\varphi, \end{cases} \tag{3.8}$$

where $A_{1n} = \dfrac{1}{\left(J_2(\chi_{1n})\sqrt{2\pi(\chi_{1n}^2 - 1)}\right)a}$ is the normalizing factor, χ_{1n} is the nth root of the equation $J_1(\chi) = 0$.

Similarly, using expression (3.3) and the reference integral given above, we obtain the expression for the field components of these modes in the diffraction zones:

$$\begin{cases} E_x(\vec{r}) = \dfrac{z(ikr-1)}{r^3} e^{ikr} A_{1n} \sin 2\beta \int_0^a J_2\left(\dfrac{\chi_{1n}\rho_0}{a}\right) J_2\left(\dfrac{k\rho\rho_0}{r}\right) e^{ik\frac{\rho_0^2}{2r}} \rho_0 d\rho_0, \\ E_y(\vec{r}) = -\dfrac{z(ikr-1)}{2\pi r^3} e^{ikr} 2\pi \int_0^a \left[J_0\left(\dfrac{\chi_{1n}\rho_0}{a}\right) J_0\left(\dfrac{k\rho_0\rho}{r}\right) - J_2\left(\dfrac{\chi_{1n}\rho_0}{a}\right) \times \right. \\ \qquad \left. \times J_2\left(\dfrac{k\rho_0\rho}{r}\right) \cos 2\beta \right] e^{ik\frac{\rho_0^2}{2r}} \rho_0 d\rho_0, \\ E_z(\vec{r}) = \dfrac{ikr-1}{r^3} e^{ikr} A_{1n} \sin\beta \int_0^a \left[J_0\left(\dfrac{\chi_{1n}\rho_0}{a}\right) J_0\left(\dfrac{k\rho_0\rho}{r}\right) \rho - \right. \\ \qquad \left. - i\rho J_0\left(\dfrac{\chi_{1n}\rho_0}{a}\right) + J_2\left(\dfrac{\chi_{1n}\rho_0}{a}\right) \right] \times \\ \qquad \times \left[J_1\left(\dfrac{k\rho_0\rho}{r}\right) - \rho J_2\left(\dfrac{\chi_{1n}\rho_0}{a}\right) J_2\left(\dfrac{k\rho_0\rho}{r}\right) \right] e^{ik\frac{\rho_0^2}{2r}} \rho_0 d\rho_0. \end{cases} \tag{3.9}$$

To compare the spatial characteristics of the investigated modes and the modes of free space, we consider in the initial plane an axisymmetric Gaussian beam linearly polarized in the y direction, in which the field $E_0 = E_{0y}(\vec{r}_0, 0)\vec{y}$ in the source plane $z = 0$ has the form:

$$E_{0y}(\rho_0) = A_0 \exp\left(-\frac{\rho_0^2}{2w_{0I}^2}\right), \tag{3.10}$$

where $A_0 = \sqrt{2/\pi}\,\dfrac{1}{w_{0I}}$ is the normalizing factor, $w_{0I} = \dfrac{w'_{0I}}{a}$, w'_{0I} is the radius of the beam in terms of intensity at the e^{-1} level from its maximum value, and a is the radius of the waveguide.

Using expression (3.3), we obtain the final expression for the components of the radiation field of a Gaussian beam in free space in the form:

$$\begin{cases} E_x(\vec{r}) = 0, \\ E_y(\vec{r}) = -\dfrac{z(ikr-1)}{2\pi r^3} e^{ikr} A_0 \int_0^a e^{-\frac{\rho_0^2}{2w_{0I}^2}} e^{ik\frac{\rho_0^2}{2r}} J_0\left(\dfrac{k\rho_0\rho}{r}\right)\rho_0 d\rho_0, \\ E_z(\vec{r}) = -\dfrac{(ikr-1)}{r^3} e^{ikr} A_0 \sin\beta \times \\ \qquad \times \int_0^a e^{-\frac{\rho_0^2}{2w_{0I}^2}} \left[\rho J_0\left(\dfrac{k\rho_0\rho}{r}\right) + i\rho_0 J_1\left(\dfrac{k\rho_0\rho}{r}\right)\right] e^{ik\frac{\rho_0^2}{2r}} \rho_0 d\rho_0. \end{cases} \quad (3.11)$$

3.2.2. Comparison of Experimental and Numerical Results

Using the obtained expressions, the transverse distributions of the intensities of the waveguide modes during their propagation in free space were calculated. The calculation was performed for lower symmetric azimuthally (TE_{0n}) and radially (TM_{0n}) polarized modes and asymmetric (TE_{1n}) modes.

Experimental studies of the propagation of terahertz laser radiation in free space were carried out on the equipment, the structural diagram of which was given earlier in chapter 2 (Fig. 2.10). The laser resonator is formed by a hollow metal waveguide with a diameter of 19.92 mm and mirrors *17, 18*. Mirror *17* is similar to the one described above, mirror *18* is mirror **II** (azimuthally symmetric diffraction grating with the parameters given in section 3. The radiation wavelength was chosen in the terahertz range λ= 0.4326 mm (generation line of a laser with optical pumping on the HCOOH molecule).

Figure 3.1 presents the experimental and calculated dependences of the half-width of the transverse distributions of intensity w at the level of $1/e^2$ on its maximum value for waveguide modes when the parameter ε, the inverse Fresnel number, changes ($\varepsilon = 1/N$, $N = a^2/\lambda L_1$, L_1 is the distance from the output end of the waveguide to the observation plane). The dependence for a Gaussian beam with a radius in the output plane of w = 8.56 mm, equal to the half-width of the TE_{01} waveguide mode at the open end of the waveguide at the $1/e^2$ level from the maximum intensity, is given here.

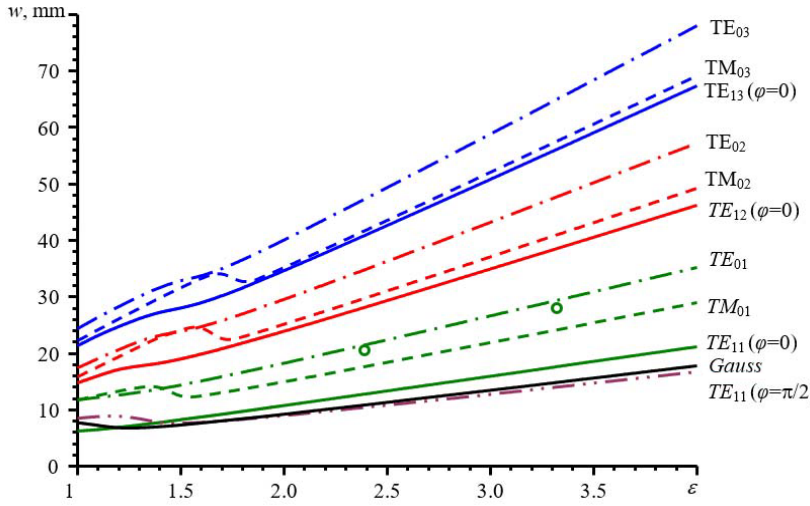

Figure 3.1. Calculated dependences of the half-width of the transverse intensity distributions *w* of the waveguide modes in free space when the parameter *ε* changes. Circles are an experiment

It can be seen from the given dependences that for small values of ε the changes in the width of the beams are nonlinear. In this region, the spatial transverse distribution of modes changes significantly (Figures 3.2 – 3.3).

The calculated and experimentally measured transverse intensity distributions of TE_{01} mode at a distance of 15 cm (ε = 0.65) and 100 cm (ε = 4.36) from the laser output mirror are shown in Figgure 3.4. A good coincidence of the experimental and calculated curves is observed. Experimentally measured by the method of two intersections (points in Figure 3.1), the TE_{01} mode divergence of an optically pumped metal waveguide laser with the wavelength and waveguide radius given above is 0.035 rad. Good agreement was obtained between the measured and calculated beam divergences for the TE_{01} mode. For comparison, Figure 3.1 shows the dependence of the half-width of a Gaussian beam with a radius in the output plane equal to the half-width of the TE_{01} waveguide mode (w = 8.56 mm) at the open end of the waveguide, calculated according to formula (3.11).

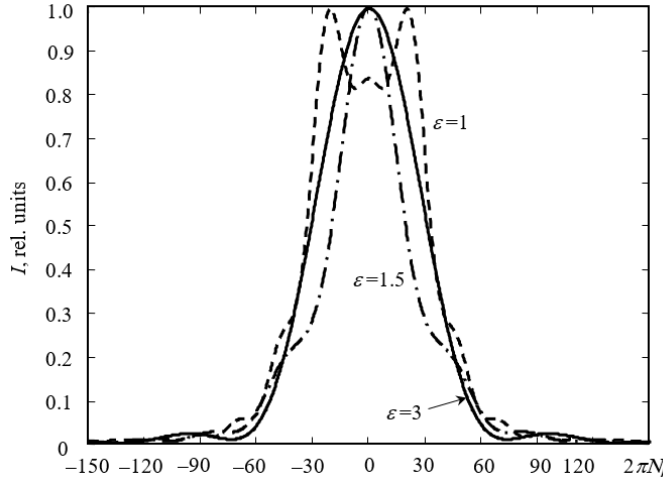

Figure 3.2. Relative transverse distributions of TE_{11} mode intensities at φ = 0

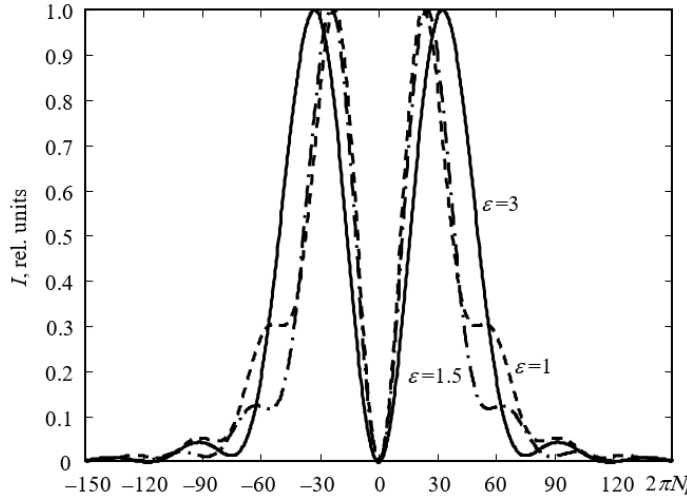

Figure 3.3. Relative transverse distributions of TM_{01} mode intensities

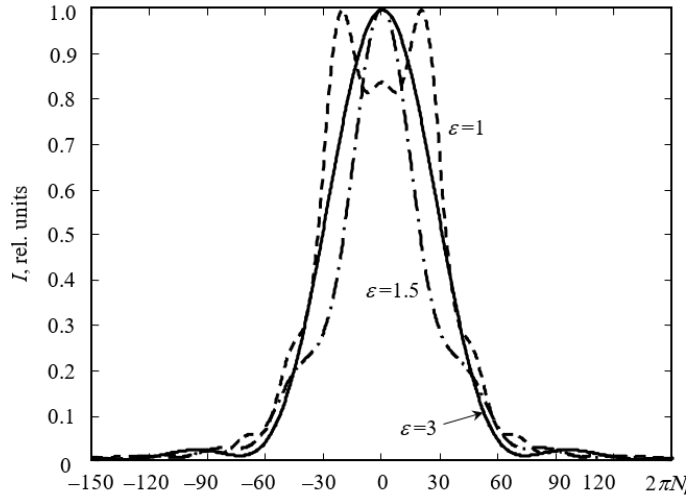

Figure 3.4. Relative transverse distributions of TE_{11} mode intensities at φ = 0

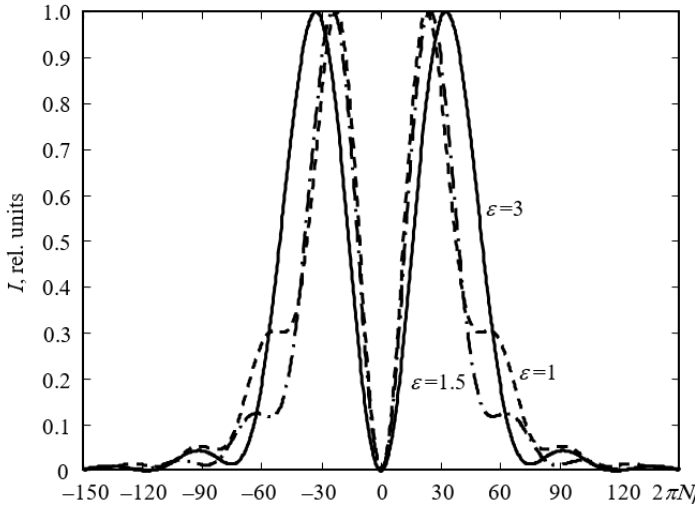

Figure 3.5. Relative transverse distributions of TM_{01} mode intensities

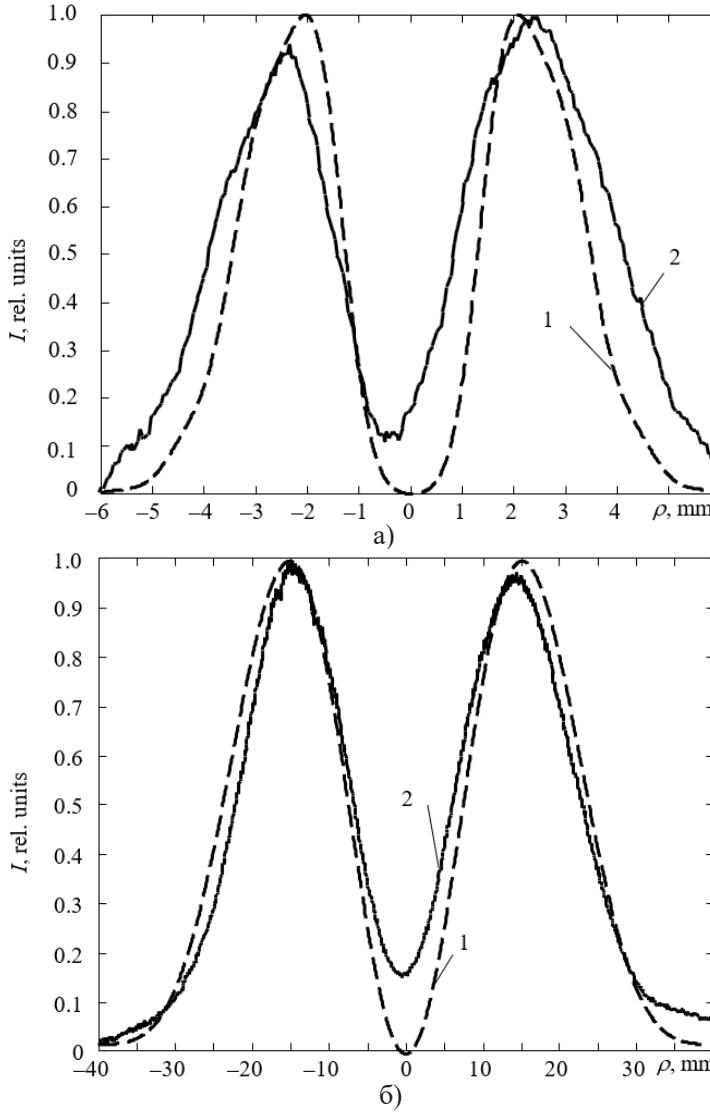

Figure 3.6. Calculated (1) and experimental (2) radial distributions of TE_{01} mode field intensity at a distance of 15 cm (a) and 100 cm (b) from the laser output mirror

The angular divergence of the Gaussian beam calculated from the obtained data for $\varepsilon > 2$ was 0.0188 rad, and calculated by the well-known expression $\Theta = \lambda/\pi w = 0.0161$ rad [141]. The angular divergence Θ of the waveguide modes is given in Table 3.1.

Table 3.1

Angular divergence of waveguide modes

Type of mode	TE_{01}	TE_{02}	TE_{03}	TM_{01}	TM_{02}	TM_{03}	TE_{11}	TE_{12}	TE_{13}	*Gauss*
Θ	0.037	0.061	0.084	0.031	0.053	0.075	0.029	0.049	0.065	0.019

The conducted theoretical and experimental comparison of the divergence of the TE_{01} mode and the Gaussian beam allows us to conclude that the obtained analytical expressions in the nonparaxial approximation correctly describe the propagation of the modes of the metal waveguide resonator in free space. A stable field structure for symmetric and asymmetric modes in the terahertz range is observed at closer distances, in contrast to the distances predicted by the well-known criterion for the far diffraction zone.

3.3. PROPAGATION OF RADIATION OF TERAHERTZ LASER BASED ON A HOLLOW DIELECTRIC CIRCULAR WAVEGUIDE IN DIFFERENT DIFFRACTION ZONES

3.3.1. Theoretical Relations

We use the previously obtained expressions (3.3) in a cylindrical coordinate system [116; 142] to study the propagation in free space of the modes of a terahertz laser based on a circular dielectric waveguide. Let the given radiation in the initial plane be in the form of symmetric azimuthally, radially and linearly polarized TE_{0n}, TM_{0n}, EH_{1n} and asymmetric linearly polarized $TE_{0n} + TH_{2n}$, $EH_{-1n} + EH_{3n}$ (n = 1, 2) modes of a circular hollow dielectric waveguide of radius a, the components of electromagnetic fields of which in the source plane $z = 0$ have a known form [50]. For TE_{0n} modes, the transverse components of the electromagnetic fields have the form:

$$\begin{cases} E_x^0\left(\vec{r_0},0\right) = -A_{0n}J_1\left(\dfrac{U_{0n}\rho_0}{a}\right)\sin\varphi, \\ E_y^0\left(\vec{r_0},0\right) = A_{0n}J_1\left(\dfrac{U_{0n}\rho_0}{a}\right)\cos\varphi, \end{cases} \tag{3.12}$$

where U_{0n} is the nth root of the equation $J_1(U_{0n}) = 0$, $A_{0n} = \dfrac{1}{\sqrt{\pi}\left|J_2(U_{0n})\right|a}$ is the normalizing factor.

For TM_{0n} modes, the transverse components of the electromagnetic fields have the following form:

$$\begin{cases} E_x^0\left(\vec{r_0},0\right) = A_{0n}J_1\left(\dfrac{U_{0n}\rho_0}{a}\right)\cos\varphi, \\ E_y^0\left(\vec{r_0},0\right) = A_{0n}J_1\left(\dfrac{U_{0n}\rho_0}{a}\right)\sin\varphi, \end{cases} \tag{3.13}$$

Transverse components of electromagnetic fields for EH_{1n} modes are presented in the following form:

$$\begin{cases} E_x^0\left(\vec{r_0},0\right) = A_{1n}J_0\left(\dfrac{U_{1n}\rho_0}{a}\right)\sin\varphi, \\ E_y^0\left(\vec{r_0},0\right) = A_{1n}J_0\left(\dfrac{U_{1n}\rho_0}{a}\right)\cos\varphi, \end{cases} \tag{3.14}$$

where U_{1n} is the nth root of the equation $J_0(U_{1n}) = 0$, $A_{1n} = \dfrac{1}{\sqrt{\pi}\left|J_1(U_{1n})\right|a}$ is the normalizing factor.

For TE_{0n} + EH_{2n} mode, the transverse components of the electromagnetic fields have the form:

$$\begin{cases} E_x^0\left(\vec{r_0},0\right) = 0, \\ E_y^0\left(\vec{r_0},0\right) = A_{2n}J_0\left(\dfrac{U_{0n}\rho_0}{a}\right)\cos\varphi, \end{cases} \tag{3.15}$$

where $A_{2n} = \dfrac{\sqrt{2}}{\sqrt{\pi}\left|J_2(U_{0n})\right|a}$ is the normalizing factor.

For the EH_{-1n} + EH_{3n} modes, the transverse components of the field are obtained as the sum of the corresponding components of the EH_{-1n} and EH_{3n} modes:

$$\begin{cases} E_x^0\left(\vec{r_0},0\right) = A_{3n}\left[1+(-1)^n\right]J_{n+1}\left(\dfrac{U_{3n}\rho_0}{a}\right)\sin\left[(n+1)\varphi\right], \\ E_y^0\left(\vec{r_0},0\right) = A_{3n}\left[1-(-1)^n\right]J_{n+1}\left(\dfrac{U_{3n}\rho_0}{a}\right)\cos\left[(n+1)\varphi\right], \end{cases} \tag{3.16}$$

where $A_{3n} = \dfrac{\sqrt{2}}{\sqrt{\pi}\left|J_2(U_{3n})\right|a}$ is the normalizing factor.

Using formula (3.3) for description the components of the electric field intensity vector that propagates, we obtain expressions for the transverse and longitudinal components of the field in an arbitrary plane $z = z_1$ in free space. For TE_{0n} mods, they look like this:

$$\begin{cases} E_x\left(\vec{r}\right) = \dfrac{-iz_1(ikr-1)}{r^3}e^{ikr}\times \\ \qquad \times A_{0n}\sin\beta\int_0^a J_1\left(\dfrac{U_{0n}\rho_0}{a}\right)\exp\left(ik\dfrac{\rho_0^2}{2r}\right)J_1\left(\dfrac{k\rho_0\rho}{r}\right)\rho_0 d\rho_0, \\ E_x\left(\vec{r}\right) = \dfrac{iz_1(ikr-1)}{r^3}e^{ikr}\times \\ \qquad \times A_{0n}\cos\beta\int_0^a J_1\left(\dfrac{U_{0n}\rho_0}{a}\right)\exp\left(ik\dfrac{\rho_0^2}{2r}\right)J_1\left(\dfrac{k\rho_0\rho}{r}\right)\rho_0 d\rho_0, \\ E_z\left(\vec{r}\right) = 0 \end{cases} \tag{3.17}$$

Similarly, the expressions for the field components of the TM_{0n} modes are obtained:

$$\begin{cases} E_x(\vec{r}) = \dfrac{iz_1(ikr-1)}{r^3} e^{ikr} \times \\ \quad \times A_{0n}\cos\beta \int_0^a J_1\left(\dfrac{U_{0n}\rho_0}{a}\right)\exp\left(ik\dfrac{\rho_0^2}{2r}\right)J_1\left(\dfrac{k\rho_0\rho}{r}\right)\rho_0 d\rho_0, \\ E_x(\vec{r}) = \dfrac{iz_1(ikr-1)}{r^3} e^{ikr} \times \\ \quad \times A_{0n}\sin\beta \int_0^a J_1\left(\dfrac{U_{0n}\rho_0}{a}\right)\exp\left(ik\dfrac{\rho_0^2}{2r}\right)J_1\left(\dfrac{k\rho_0\rho}{r}\right)\rho_0 d\rho_0, \\ E_z(\vec{r}) = \dfrac{(ikr-1)}{r^3} e^{ikr} A_{0n}\sin\beta \int_0^a J_1\left(\dfrac{U_{0n}\rho_0}{a}\right)\exp\left(ik\dfrac{\rho_0^2}{2r}\right)\times \\ \quad \times\left[\rho_0 J_0\left(\dfrac{k\rho_0\rho}{r}\right) + i\rho J_1\left(\dfrac{k\rho_0\rho}{r}\right)\right]\rho_0 d\rho_0. \end{cases} \tag{3.18}$$

The expressions for the components field of the EH_{1n} modes have the following form:

$$\begin{cases} E_x(\vec{r}) = 0, \\ E_y(\vec{r}) = \dfrac{-z_1(ikr-1)}{r^3} e^{ikr} A_{1n} \int_0^a J_0\left(\dfrac{U_{1n}\rho_0}{a}\right)\exp\left(ik\dfrac{\rho_0^2}{2r}\right)J_0\left(\dfrac{k\rho_0\rho}{r}\right)\rho_0 d\rho_0, \\ E_z(\vec{r}) = \dfrac{(ikr-1)}{r^3} e^{ikr} A_{1n}\sin\beta \int_0^a J_0\left(\dfrac{U_{1n}\rho_0}{a}\right)\exp\left(ik\dfrac{\rho_0^2}{2r}\right)\times \\ \quad \times\left[\rho J_0\left(\dfrac{k\rho_0\rho}{r}\right) + i\rho_0 J_1\left(\dfrac{k\rho_0\rho}{r}\right)\right]\rho_0 d\rho_0. \end{cases} \tag{3.19}$$

For TE_{0n} + EH_{2n} modes the transverse and longitudinal components of the field are expressed in the following form:

$$\begin{cases} E_x(\vec{r}) = 0, \\ E_y(\vec{r}) = \dfrac{iz_1(ikr-1)}{r^3} e^{ikr} \cos(\beta) A_{1n} \int_0^a J_0\left(\dfrac{U_{0n}\rho_0}{a}\right) \exp\left(ik\dfrac{\rho_0^2}{2r}\right) J_0\left(\dfrac{k\rho_0\rho}{r}\right) \rho_0 d\rho_0, \\ E_z(\vec{r}) = \dfrac{(ikr-1)}{r^3} e^{ikr} A_{1n} \sin(2\beta) \int_0^a J_1\left(\dfrac{U_{0n}\rho_0}{a}\right) \exp\left(ik\dfrac{\rho_0^2}{2r}\right) \times \\ \quad \times \left[\rho_0 J_2\left(\dfrac{k\rho_0\rho}{r}\right) - i\rho J_1\left(\dfrac{k\rho_0\rho}{r}\right)\right] \rho_0 d\rho_0. \end{cases} \tag{3.20}$$

For the $EH_{-1n} + EH_{3n}$ modes the transverse and longitudinal components of the field have the form:

$$\begin{cases} E_x(\vec{r}) = \dfrac{-z_1(ikr-1)}{r^3} e^{ikr} \left[1+(-1)^n\right]\left[(-i)^{n+1}\right] \sin\left[(n+1)\beta\right] \times \\ \quad \times \int_0^a J_{n+1}\left(\dfrac{U_{1n}\rho_0}{a}\right) J_{n+1}\left(\dfrac{k\rho_0\rho}{r}\right) e^{ik\frac{\rho_0^2}{2r}} \rho_0 d\rho_0, \\ E_y(\vec{r}) = \dfrac{-z_1(ikr-1)}{r^3} e^{ikr} \left[1-(-1)^n\right]\left[(-i)^{n+1}\right] \cos\left[(n+1)\beta\right] \times \\ \quad \times \int_0^a J_{n+1}\left(\dfrac{U_{1n}\rho_0}{a}\right) J_{n+1}\left(\dfrac{k\rho_0\rho}{r}\right) e^{ik\frac{\rho_0^2}{2r}} \rho_0 d\rho_0, \\ E_z(\vec{r}) = E_{z_1}(\vec{r}) + E_{z_{20}}(\vec{r}) + E_{z_{21}}(\vec{r}) + E_{z_3}(\vec{r}) + E_{z_{40}}(\vec{r}) + E_{z_{41}}(\vec{r}), \end{cases} \tag{3.21}$$

where

$$E_{z_1}(\vec{r}) = \frac{(ikr-1)}{r^3} e^{ikr} \left[1-(-1)^n\right]\left[(-i)^{n+1}\right] \sin\left[(n+1)\beta\right] \rho\cos(\beta) \times$$
$$\times \int_0^a J_{n+1}\left(\frac{U_{1n}\rho_0}{a}\right) J_{n+1}\left(\frac{k\rho_0\rho}{r}\right) e^{ik\frac{\rho_0^2}{2r}} \rho_0 d\rho_0,$$
$$E_{z_{20}}(\vec{r}) = \left[\frac{-(ikr-1)}{2r^3} e^{ikr}\right]\left[1-(-1)^n\right]\left[(-i)^n\right] \sin(\beta) \times$$
$$\times \int_0^a J_{n+1}\left(\frac{U_{1n}\rho_0}{a}\right) J_n\left(\frac{k\rho_0\rho}{r}\right) e^{ik\frac{\rho_0^2}{2r}} \rho_0^2 d\rho_0,$$

$$E_{z_{21}}(\vec{r}) = \left[\frac{-(ikr-1)}{2r^3}e^{ikr}\right]\left[1-(-1)^n\right]\left[(-i)^{n+2}\right]\sin\left[(n+2)\beta\right]\times$$

$$\times\int_0^a J_{n+1}\left(\frac{U_{1n}\rho_0}{a}\right)J_{n+2}\left(\frac{k\rho_0\rho}{r}\right)e^{ik\frac{\rho_0^2}{2r}}\rho_0^2 d\rho_0,$$

$$E_{z3}(\vec{r}) = \left[\frac{(ikr-1)}{r^3}e^{ikr}\right]\left[1-(-1)^n\right]\left[(-i)^{n+1}\right]\cos\left[(n+1)\beta\right]\rho\sin(\beta)\times$$

$$\times\int_0^a J_{n+1}\left(\frac{U_{1n}\rho_0}{a}\right)J_{n+1}\left(\frac{k\rho_0\rho}{r}\right)e^{ik\frac{\rho_0^2}{2r}}\rho_0 d\rho_0,$$

$$E_{z_{40}}(\vec{r}) = \left[\frac{-(ikr-1)}{2r^3}e^{ikr}\right]\left[1-(-1)^n\right]\left[(-i)^{n+2}\right]\sin\left[(n+2)\beta\right]\rho\cos(\beta)\times$$

$$\times\int_0^a J_{n+1}\left(\frac{U_{1n}\rho_0}{a}\right)J_{n+2}\left(\frac{k\rho_0\rho}{r}\right)e^{ik\frac{\rho_0^2}{2r}}z_1\rho_0^2 d\rho_0,$$

$$E_{z_{41}}(\vec{r}) = \left[\frac{(ikr-1)}{2r^3}e^{ikr}\right]\left[1-(-1)^n\right]\left[(-i)^{n}\right]\sin(\beta)\times$$

$$\times\int_0^a J_{n+1}\left(\frac{U_{1n}\rho_0}{a}\right)J_{n}\left(\frac{k\rho_0\rho}{r}\right)e^{ik\frac{\rho_0^2}{2r}}\rho_0^2 d\rho_0.$$

To compare the spatial characteristics of the investigated modes and the modes of free space, we consider in the initial plane an axisymmetric Gaussian beam linearly polarized in the *y* direction, in which the field $E_0 = E_{0y}\left(\vec{r_0},0\right)\vec{j}$ in the source plane $z = 0$ has the form:

$$E_{0y}(\rho_0) = A_0\exp\left(-\frac{\rho_0^2}{2w_{0I}^2}\right), \tag{3.22}$$

where $A_0 = \sqrt{2/\pi}\,\frac{1}{w_{0I}}$ is the normalization factor, $w_{0I} = \frac{w'_{0I}}{a}$, w'_{0I} is the radius of the beam in terms of intensity at the e^{-1} level from its maximum value, and *a* is the radius of the waveguide.

Using expression (3.3), we obtain the final expression for the components of the Gaussian beam radiation field in the form:

$$\begin{cases} E_x\left(\vec{r}\right)=0, \\ E_y\left(\vec{r}\right)=-\dfrac{z(ikr-1)}{2\pi r^3}e^{ikr}A_0\int_0^a e^{-\frac{\rho_0^2}{2w_{0I}^2}}e^{ik\frac{\rho_0^2}{2r}}J_0\left(\dfrac{k\rho_0\rho}{r}\right)\rho_0 d\rho_0, \\ E_z\left(\vec{r}\right)=-\dfrac{(ikr-1)}{r^3}e^{ikr}A_0\sin\beta\times \\ \qquad\times\int_0^a e^{-\frac{\rho_0^2}{2w_{0I}^2}}\left[\rho J_0\left(\dfrac{k\rho_0\rho}{r}\right)+i\rho_0 J_1\left(\dfrac{k\rho_0\rho}{r}\right)\right]e^{ik\frac{\rho_0^2}{2r}}\rho_0 d\rho_0. \end{cases} \tag{3.23}$$

3.3.2. Comparison of Experimental and Numerical Results

Experimental studies of the propagation of THz laser radiation in free space were carried out on the setup, the structural diagram of which is given in section 2 (see Fig. 2.10). The laser resonator is formed by a hollow dielectric waveguide with a diameter of $2a$ = 35 mm and mirrors *17*, *18*. The output mirror *18* was mirror **II**, made in the form of an azimuthally symmetric diffraction grating with the parameters given in section 2. Calculations and experiments were carried out at a wavelength of 0.4326 mm.

Using the obtained expressions, we calculated the transverse distributions of the field intensity of laser beams excited by symmetric azimuthally, radially and linearly polarized TE_{0n}, TM_{0n}, EH_{1n} and asymmetric linearly polarized $TE_{0n}+EH_{2n}$, $EH_{-1n}+EH_{3n}$ (n = 1, 2) modes of the dielectric waveguide resonator of a terahertz laser during their propagation in free space in near and far diffraction zones. Figures 3.7 – 3.12 show the transverse distributions of the field intensity of the given modes at different distances from the laser resonator.

Figure 3.13 presents the experimental and calculated dependences of the half-width of the transverse intensity distributions at the level of $1/e^2$ on its maximal value for waveguide modes when the parameter ε, the inverse Fresnel number, changes. It can be seen that when $\varepsilon < 2$, the transverse distribution of the mode intensity changes significantly. In the region $\varepsilon > 2$, the transverse profiles of the radiation beams acquire a stable structure, and only their width changes when ε increases.

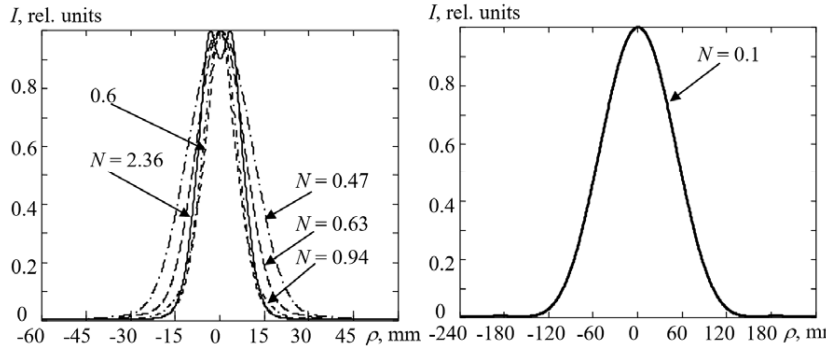

a) b)

Figure 3.7. Transverse distributions of field intensity EH_{11} mode: a) in the near diffraction zone; b) in the far zone of diffraction

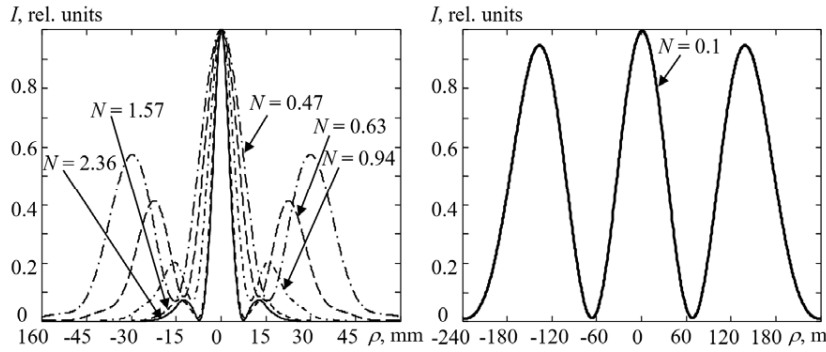

a) b)

Figure 3.8. Transverse distributions of field intensity EH_{12} mode: a) in the near diffraction zone; b) in the far zone of diffraction

There is good agreement between experimentally measured (points in Figure 3.13) and calculated data for radiation beams excited by EH_{11}, TE_{01}+EH_{21} modes. For comparison, the figure shows the dependence of the half-width of the Gaussian beam on the parameter ε. The radius of the beam is chosen equal to the radius of the EH_{11} mode at the $1/e^2$ level from its maximum value at the output end of the waveguide.

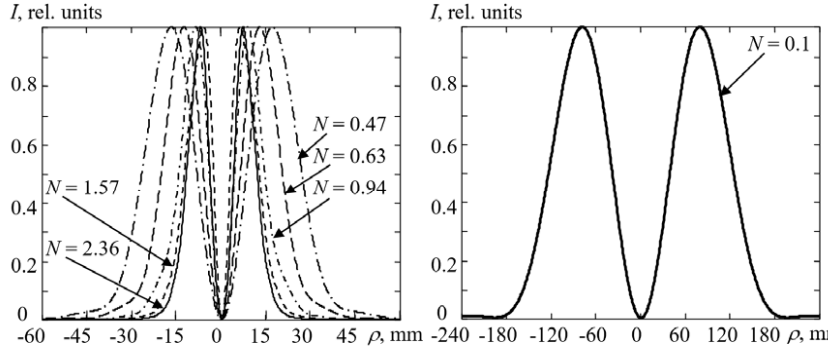

Figure 3.9. Transverse distributions of field intensity TE_{01}, TM_{01}, $TE_{01}+EH_{21}$ modes: a) in the near diffraction zone; b) in the far zone of diffraction

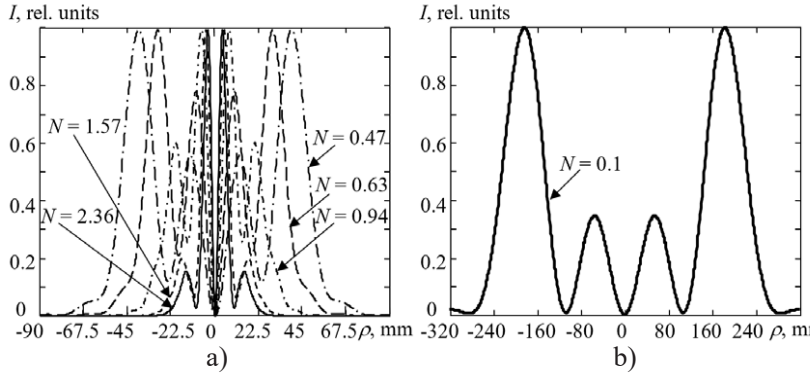

Figure 3.10. Transverse distributions of field intensity TE_{02}, TM_{02}, $TE_{02}+EH_{22}$ modes: a) in the near diffraction zone; b) in the far zone of diffraction

The experimentally obtained and calculated values of the divergence of laser beams in the far zone, obtained by the method of focal spot, for the modes EH_{11} and $TE_{01}+EH_{21}$ within the measurement error coincide and are shown in Table 3.2, where the calculated divergencies for other waveguide modes and the Gaussian beam are also given.

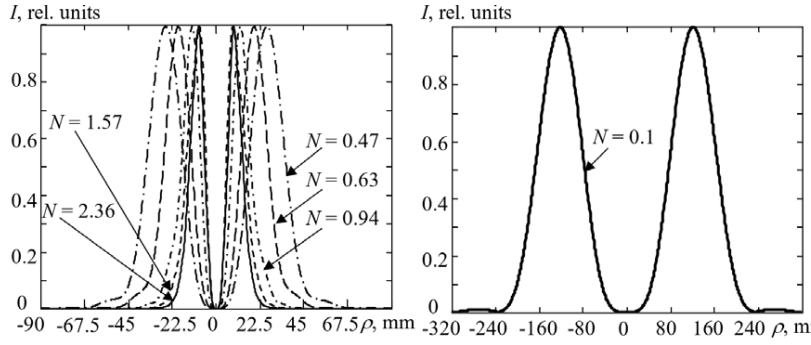

Figure 3.11. Transverse distributions of field intensity $EH_{-11}+EH_{31}$ modes: a) in the near diffraction zone; b) in the far zone of diffraction

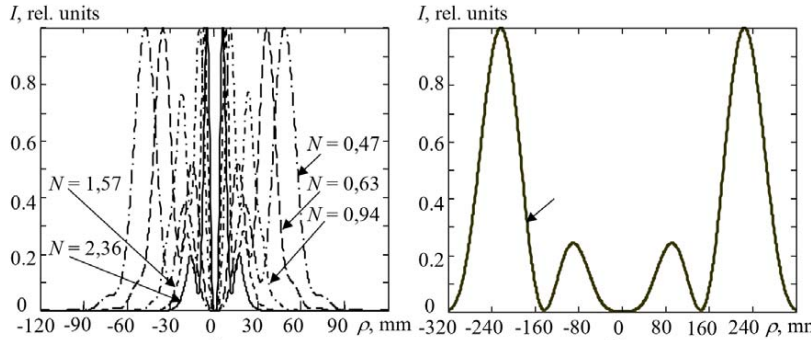

Figure 3.12. Transverse distributions of field intensity $EH_{-12}+EH_{32}$ modes: a) in the near diffraction zone; b) in the far zone of diffraction

Table 3.2

Calculated divergencies of waveguide modes and Gaussian beam

Waveguide modes	TE_{01} TE_{02}	TM_{01} TM_{02}	EH_{11} EH_{12}	$TE_{01}+EH_{21}$ $TE_{02}+EH_{22}$	$EH_{-11}+EH_{31}$ $EH_{-12}+EH_{32}$	Gaussian beam
Angular divergence Θ, rad.	0.0212 0.0334	0.0212 0.0334	0.0131 0.0293	0.0212 0.0334	0.0289 0.0371	0.011

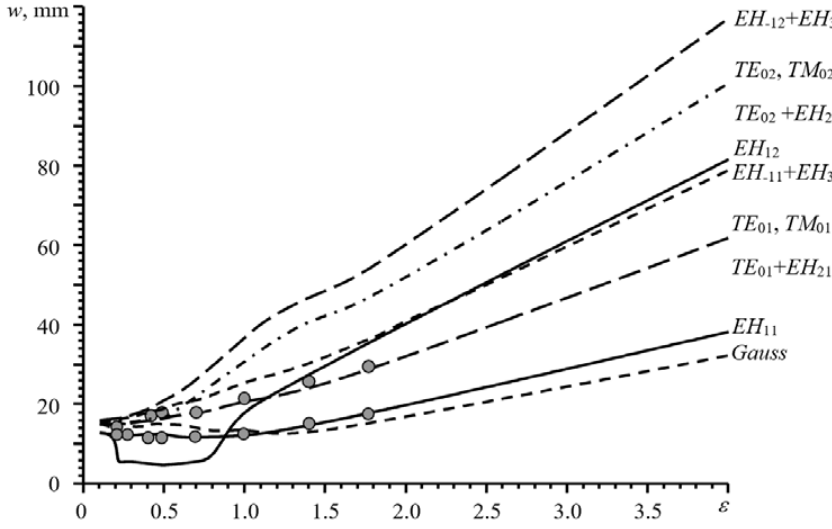

Figure 3.13. Calculated dependences of the half-width of the transverse intensity distributions *w* of the waveguide modes in free space when the parameter *ε*

These results allow us to conclude that the obtained analytical expressions in the nonparaxial approximation correctly describe the propagation of laser beams excited by the modes of the dielectric resonator of a terahertz laser with a circular waveguide in free space. At the same time, a stable field structure in free space for dielectric resonator modes in the terahertz range is observed at closer distances from the end of the waveguide ($L \geq 2a^2 / \lambda$)in contrast to the distances predicted by the well-known criterion ($L \geq 8a^2 / \lambda$) for the far diffraction zone [143].